Advances in surface passivation of nanoscale zerovalent iron (NZVI): A critical review

Sungjun Bae,[†] Richard N. Collins,[‡] T. David Waite[‡] and Khalil Hanna*[,§]

[†]Department of Civil and Environmental Engineering, Konkuk University, 120 Neungdong-ro, Gwangjin-gu, Seoul 05029, Republic of Korea

[‡]School of Civil and Environmental Engineering, University of New South Wales, Sydney, New South Wales 2052, Australia

[§] Univ Rennes, Ecole Nationale Supérieure de Chimie de Rennes, CNRS, ISCR – UMR6226, F-35000 Rennes, France

*Corresponding author: Tel.: +33 2 23 23 80 27; fax: +33 2 23 23 81 20.

E-mail address: khalil.hanna@ensc-rennes.fr (K. Hanna)

A revised review submitted to *Environmental Science and Technology*

September, 2018

ABSTRACT

Nanoscale zerovalent iron (NZVI) is one of the most extensively studied nanomaterials in the fields of wastewater treatment and remediation of soil and groundwater. However, rapid oxidative transformations of NZVI can result in reduced NZVI reactivity. Indeed, the surface passivation of NZVI is considered one of the most challenging aspects in successfully applying NZVI to contaminant degradation. The oxidation of NZVI can lead to the formation of Fe^{II}-bearing phases (e.g., $Fe^{II}O$, $Fe^{II}(OH)_2$, $Fe^{II}Fe^{III}{}_2O_4$) on the NZVI surface or complete oxidation to ferric (oxyhydr)oxides (e.g., $Fe^{III}OOH$). This corrosion phenomenon is dependent upon various factors including the composition of NZVI itself, the type and concentration of aqueous species, reaction time and oxic/anoxic environments. As such, the co-existence of different Fe oxidation states on NZVI surfaces may also, in some instances, provide a unique reactive microenvironment to promote the adsorption of contaminants and their subsequent transformation via redox reactions. Thus, an understanding of passivation chemistry, and its related mechanisms, is essential not only for effective NZVI application but also for accurately assessing the positive and negative effects of NZVI surface passivation. The aim of this review is to discuss the nature of the passivation processes that occur and the passivation byproducts that form in various environments. In particular, the review presents: i) the strengths and limitations of state-of-the-art techniques (e.g., electron microscopies and X-ray based spectroscopies) to identify passivation byproducts; ii) the passivation mechanisms proposed to occur in anoxic and oxic environments; and iii) the effects arising from synthesis procedures and the presence of inorganics/organics on the nature of the passivation byproducts that form. In addition, several depassivation strategies that may assist in increasing and/or maintaining the reactivity of NZVI are considered, thereby enhancing the effectiveness of NZVI in contaminant degradation.

1. INTRODUCTION

In recent decades, zerovalent iron (ZVI, Fe(0)) has been extensively studied for its capacity to transform contaminants in soils, groundwater and industrial wastewaters because of: (i) its ability to reductively transform a wide variety of compounds, such as halogenated organics, into less toxic and/or more biodegradable forms; (ii) the abundance of iron (the fourth most abundant element in the earth's crust); (iii) the relative environmental friendliness of an iron-based technology compared to other zerovalent metals (such as Mn(0) and Cu(0)) and (iv) the low cost of Fe^0 mass production.[1–7] In particular, nanoscale zerovalent iron (NZVI) has attracted attention due to the potential advantages arising from high particle reactivity (resulting from the small size and high surface area of NZVI) when compared to ZVI.[3–6,8–21] Moreover, NZVI has been confirmed to reductively remove various organic (e.g., chlorinated aliphatic[3,6,8–10] and aromatic compounds[10,11,13,14]), inorganic (e.g., nitrate,[12] Cr(VI),[17] As(III)[18–22] and Cd(II)[23]) and radioactive (e.g., U(VI)[24–26] and Tc(VII)[27]) contaminants under anoxic conditions. It has also been demonstrated that NZVI can induce the oxidative degradation of organic contaminants (e.g., pharmaceuticals[28,29] and herbicides[30,31]). This may occur as a result of the reduction of dissolved oxygen (O_2) and the associated production of hydrogen peroxide (H_2O_2) that subsequently reacts with Fe(II) (that is also produced during oxidation) leading to initiation of the Fenton reaction ($Fe(II) + H_2O_2 \rightarrow Fe(III) + HO^* + OH^-$) and the generation of strongly oxidizing hydroxyl radicals (HO^*, 2.80 V).

Typical NZVI particles have a core-shell (Fe(0)-Fe (oxyhydr)oxide) structure with the spherical nanosized primary particles forming chain-like aggregates with sizes ranging up to a few micrometers.[3] Moreover, the aggregates exhibit the magnetic properties of the primary particles with the magnetism of the primary particles influencing the size and structure of these assemblages.[32] The co-existence of the Fe(0) core and oxidized Fe surface layer provides a unique reactive surface for the initial adsorption of contaminants and their

subsequent transformation on the particle surface via reductive or oxidative pathways.[3,5,14,16,29,30] In accordance with contaminant adsorption, oxidation or reduction, Fe may undergo oxidation (from Fe(0) to Fe(II) and Fe(II) to Fe(III)), precipitation (as Fe(II) and/or Fe(III) solids) and, possibly, co-precipitation with ionic species.[8,33–35] Concomitantly, it may also be necessary to consider reactions with other solution phase entities such as O_2, (which, as noted above, may be reduced to H_2O_2, possibly due to adsorption to NZVI or its (oxyhydr)oxide-coated surface),[28,29] sulfate (which may possibly be reduced to sulfide, resulting in the formation of FeS solid phases on the NZVI surface)[35] and carbonate (which may also promote the precipitation of ferrous carbonate minerals).[36]

Many researchers have demonstrated that NZVI undergoes surface oxidation (or surface passivation) when used for the removal of contaminants in variably oxic environments.[3,6,8,29] In addition, a field study has shown that 78–97% of Fe(0) injected was oxidized in a sediment sample after 165 d at a remedial site contaminated with a dense non-aqueous phase liquid (DNAPL). [37] Investigations have revealed that, depending on the environmental conditions and types of contaminants present, NZVI surface layers (and eventually, the bulk of the solid) transform to different Fe mineral phases, such as vivianite ($Fe^{II}_3(PO_4)_2 \cdot 8H_2O$), $Fe(OH)_2$, green rust (Fe(II)-Fe(III) layered double hydroxides with various interlayer anions (e.g. Cl^-, SO_4^{2-} and CO_3^{2-})), ferrihydrite, magnetite ($Fe^{II}{}_1{}^{III}{}_2O_4$), lepidocrocite ($\gamma$-$Fe^{III}OOH$), goethite ($\alpha$-$Fe^{III}OOH$), mackinawite ($Fe^{II}S$), and siderite ($Fe^{II}CO_3$), as presented in Table 1. Moreover, NZVI can be completely transformed to lepidocrocite in oxygenated water[38] and partially transformed to $Fe(OH)_2$ in O_2-free water in the absence of contaminants.[39] The passivation kinetics and the nature of the products generated have a significant influence on the long-term viability of the technology given that Fe(II)-containing minerals such as magnetite,[40–43] vivianite,[44–47] and green rust[48–50] and surface-bound Fe(II)[51,52] can further remove organic and inorganic contaminants. In addition, Fe(III)-containing minerals (e.g., maghemite (γ-Fe_2O_3),[53]

goethite[54] and hematite[55]) can effectively remove contaminants via sorptive effects. For example, it has been reported that, in anoxic conditions, passivated NZVI demonstrated similar or slightly higher sorptive ability for perfluoroalkyl acids[56] and As(V)[57] when compared to fresh NZVI. These results are most likely due to the presence of a greater number of adsorption sites on the Fe (oxyhydr)oxides passivating the NZVI surface compared to the number of sites on pristine NZVI. These findings imply that passivation byproducts of NZVI can potentially act as reactants for the further removal of contaminants, even after the depletion of the initial NZVI.

Although the positive effects of passivation are evident, there are several adverse effects to the formation of passivation byproducts on NZVI that should be considered (in addition to reduced activity). The production of reactive oxygen species (ROS) in NZVI suspensions, as previously mentioned, was considered to account for the high toxicity of fresh NZVI to rodent neuron and microglia cells when compared to the limited effect of aged NZVI and magnetite nanoparticles[58] with the severity of toxicity related to the iron oxidation state with Fe(0) > Fe(II) > Fe(III).[59] The toxicity of passivation byproducts from NZVI may be lower than that of NZVI however the results of the above studies suggest that the passivation byproducts (i.e., Fe(II) and Fe(III) species) can also induce secondary toxic effects. In addition, it has been suggested that the presence of nanoparticles may enhance the transport of contaminants associated with these nanoparticles,[60] though certain reports suggest that the mobility of NZVI particles is likely to be retarded as a result of the association of these particles with subsurface sediments.[61,62] Therefore, an understanding of passivation kinetics, transformation byproducts and related mechanisms is required when considering the reactivity, longevity and stability of NZVI.

Although a number of reviews regarding NZVI have been published, most reviews have focused on NZVI synthesis and characterization, application to the removal of contaminants

or implementation and results of field studies.[15,63–74] In comparison, in this review, we introduce: (i) common characterization techniques for determining the nature of passivation byproducts; (ii) insights into the passivation mechanism(s) underlying observed structural transformations of NZVI in oxic and anoxic environments and (iii) the effect of synthesis methods and solution conditions such as the presence of various organic and inorganic species on the passivation process. In addition, we describe various depassivation strategies that could potentially be used to either prevent or retard passivation processes and thereby extend the lifetime over which NZVI is an effective agent for the degradation of contaminants.

2. CHARACTERIZATION OF NZVI PASSIVATION BYPRODUCTS

To identify the NZVI passivation mechanism operating under specific conditions, the investigation and monitoring of the formation of passivation byproducts throughout and after the passivation process are required. In this section, common techniques used for identifying passivation byproducts are reviewed and the benefits and limitations of each technique are discussed. The primary methods of interest include electron microscopy, X-ray diffraction (XRD), X-ray photoelectron spectroscopy (XPS), Raman and Mössbauer spectroscopies and X-ray absorption spectroscopy (XAS).

2.1. Electron Microscopy

Transmission and scanning electron microscopy (TEM and SEM) have been the most widely used techniques to determine the morphological characteristics of NZVI passivation byproducts. TEM can provide visual information at the nanoscale level of properties such as the core size of fresh NZVI, the thickness of the passivating layer after partial passivation, and morphological changes after complete structural transformation. Additionally, crystallographic information including crystallinity and lattice spacing can be obtained using

149 selected area electron diffraction.[36,39] For fresh NZVI, a spherically-shaped core-shell
150 structure is commonly observed using TEM. The size of the core is typically within a range of
151 tens of nanometers with the core covered by a thin Fe (oxyhydr)oxide layer of several
152 nanometers thickness as shown in Figure S1.[3,8,19,38,75] After surface passivation,
153 morphological changes in the NZVI structure can be detected using TEM. Typical changes
154 include loss of the Fe(0) core and the appearance of hollow (oxyhydr)oxide shells with this
155 transformation reported to occur within 24 h under oxic conditions.[38] Further aging to 72 h
156 can result in the formation of flake- or acicular-shaped minerals (such as lepidocrocite).[38]
157 Another effective analytical technique typically associated with TEM is X-ray energy
158 dispersive spectroscopy (XEDS). The results of XEDS can provide the elemental composition
159 of passivation byproducts and can support identification of the Fe mineral phases present,
160 especially when certain elements such as P and S are co-localised in minerals such as
161 (respectively) vivianite ($Fe_3(PO_4)_2$) and mackinawite (FeS).[33,34,35] In recent times, scanning
162 TEM (STEM)-XEDS has been used to identify the passivation mechanism that occurs in
163 single nanoparticles by the acquisition of nanoscale images and elemental maps.[36,38,76] For
164 instance, the growth of amorphous assemblages within the NZVI core with subsequent
165 transformation to plate-like crystalline forms has been observed using STEM (Figures 1(a–c)).
166 These results can then be matched to XEDS maps to reveal a decrease and increase,
167 respectively, in the Fe and O contents within the NZVI core.[36]
168
169 **2.2. X-ray Diffraction (XRD)**
170 X-ray diffraction is one of the most popular analytical techniques for characterizing the
171 particular minerals that form upon NZVI passivation.[15] It is particularly useful for identifying
172 crystalline phases that give sharp and characteristic diffraction peak patterns. Most studies in
173 which the mineralogy of passivated NZVI has been examined by XRD have typically been

limited to analyses 'before' and 'after' reaction of the sample with very limited insight gained into the kinetics of mineral transformations.[22,77–79] A large number of iron crystalline phases have been identified by XRD in passivation byproduct studies however lepidocrocite and magnetite/maghemite are overwhelmingly the dominant phases detected.[15] The latter two minerals cannot be identified separately by XRD as both have indistinguishable diffraction patterns despite their different oxidation states. Other less common NZVI passivation byproducts detected by XRD include ferrihydrite,[77] goethite,[80] vivianite,[33,34] amakinite ($Fe^{II}(OH)_2$),[81] hematite,[18] chukanovite ($Fe^{II}_2(OH)_2CO_3$)[82] and carbonate green rust.[83]

Perhaps the most significant limitation of using XRD to identify passivation byproducts is that some minerals, including NZVI itself, quite often present as X-ray amorphous and/or only display broad diffraction peaks.[15] In addition, the mineral detection limits for XRD are in the order of 2 to 3 wt. %.[15] Thus, quantitative analysis of the relative proportions of minerals present could be difficult or impossible with this analytical approach. This could possibly explain why the very common nanocrystalline, X-ray amorphous mineral ferrihydrite has rarely been identified as a major passivation byproduct in NZVI studies in which XRD was used as the primary characterization technique.

2.3. X-ray Photoelectron Spectroscopy (XPS)

X-ray photoelectron spectroscopy is a surface sensitive technique that can be used to characterize several nanometers of the NZVI outer layer. Although it is difficult to conclusively determine the nature of the NZVI passivation byproducts using XPS due to the limited information that can be obtained on the mineral phases, this technique can provide important information on the nature of the elements present at the NZVI surface including their oxidation states. The kinetic energy and number of electrons emitted from irradiation of the surface by X-rays of known energy are measured during XPS analysis. For the

199 determination of the oxidation state of elements present within the surface layer, the narrow
200 peaks for the Fe($2p_{3/2}$) and O(1s) binding energies are particularly useful.[8,40,84] A
201 comprehensive understanding of the oxidation states of the Fe and O species on the NZVI
202 surface can provide critical information on passivation byproducts.[38,84–86] For example, the
203 presence of an Fe(0) peak at ~706 eV indicates that the core Fe(0) is preserved because XPS
204 is sensitive to the outermost layer of the particles.[6] In addition, it has been reported that after
205 72 h reaction with oxygenated water, NZVI passivation byproducts displayed peaks of Fe at
206 ~711 eV and O at ~530 eV and 531 eV, indicating the presence of Fe_2O_3, Fe_3O_4 and/or
207 FeOOH.[38]
208
209 **2.4. Raman and Mössbauer Spectroscopies**
210 Raman spectroscopy can be carried out *in situ* to monitor the formation of NZVI
211 passivation byproducts, particularly when the minerals to be identified are poorly crystalline.
212 However, the transformation of Fe (oxyhydr)oxides as a result of laser-induced thermal
213 heating may complicate interpretation of results.[77] For example, hematite is often detected by
214 Raman spectroscopy but absent in corresponding XRD data.[77,78] In the early stages of NZVI
215 aqueous oxic corrosion, wustite ($Fe^{II}O$) can be detected by Raman spectroscopy (~595 cm^{-1})[78]. It is an unstable intermediate phase generally formed in small amounts below the
217 detection limit of XRD. At longer aging times (e.g. 30 d in static deionized water or 24 h in
218 deionized water mixed at 300 rpm), Raman analyses have revealed the simultaneous co-
219 existence of maghemite (665 and 730 cm^{-1}), magnetite (670 cm^{-1}) and lepidocrocite (650 cm^{-1}).[77,78] On prolongation of NZVI aging time to 60–90 d in static water or 48-72 h in stirred
221 water, only lepidocrocite (250, 380, 526 and 650 cm^{-1}) was identified (in close agreement
222 with XRD results).[38] Raman analysis has been used to show that aging under anoxic
223 conditions favors the formation of wustite, goethite and akaganeite (β-$Fe^{III}OOH$).[78]

^{57}Fe Mössbauer spectroscopy can be used for detecting Fe atoms in different oxidation states and is a useful technique to identify the nature of any amorphous mineral phases present. Mössbauer spectroscopy can provide relevant information on the valency and spin states of Fe species as well as their magnetic properties via analysis of the hyperfine parameters. As such, magnetite and maghemite can be distinguished using this technique. Moreover, it can be used to determine the percentages of elemental Fe(0) and other secondary minerals that are present.[63] The typical ^{57}Fe Mössbauer spectrum of ZVI exhibits a single magnetic component corresponding to Fe(0) with hyperfine parameters corresponding to a cubic phase of metallic Fe. However a simple spectrum of this nature has rarely been observed for NZVI, even when the NZVI was pristine and freshly- prepared.[19,63,87] Typically, a complex hyperfine structure is observed with at least five components: a magnetic sextet with narrow lines corresponding to that of Fe(0), two quadruple components corresponding to Fe(III) and Fe(II) species, and two magnetic components. Mössbauer specialists suggest that these results are indicative of the presence of disordered ferric (oxyhydr)oxides (e.g., $Fe(OH)_3$) and/or superparamagnetic ferric oxides (e.g., Fe_3O_4) on the passivated surface of Fe(0). When NZVI reacts with contaminants in water, a quadruple doublet and a magnetic sextet with broadened lines are commonly observed and have generally been attributed to the formation of lepidocrocite and a mixture of magnetite and maghemite, respectively.[19,87]

2.5. X-ray Absorption Spectroscopy (XAS)

Despite the widespread use in the fields of geochemistry and material science, XAS has had a limited application in NZVI studies with only a handful of studies describing the use of this technique to characterization of NZVI[15,33,88,89] or NZVI passivation byproducts.[36,79,86,90–92] One of the great strengths of Fe K-edge XAS is that it can provide quantitative insight into all the iron minerals present. This is because the high energy of the Fe K-edge (7112 eV for

Fe(0)), allows for the entirety of the particles to be sampled by the beam. As an XAS spectrum is a linear combination of its components, it can then be fitted with reference material spectra in a linear least-squares fitting manner using software such as ATHENA.[93] As recommended elsewhere,[67] the choice of reference material spectra and the number of components to fit sample spectra should be guided on evidence from complementary analytical techniques, knowledge of the NZVI system, or principle component analysis and target analysis.

In the NZVI studies mentioned above, either the X-ray absorption near-edge structure (XANES) or extended X-ray absorption fine structure (EXAFS) regions of the XAS spectrum have been modelled. Generally, the Fe K-edge XANES region can be used for fitting spectra when there are multiple Fe oxidation states present.[86,89–91] However, it is a less useful region to distinguish between Fe(III) oxyhydroxide passivation byproducts. For example, the XANES spectra of ferrihydrite, lepidocrocite and goethite can, for fitting purposes, be practically identical when using a Si(111) monochromator. If the identity of the exact Fe(III) oxyhydroxides is an important component of a NZVI study, then the EXAFS region is better suited for fitting of data.[36,92] Interestingly, all the XAS studies that have examined NZVI passivation byproducts have done so under oxidative conditions. Nevertheless, as noted in many other NZVI studies, lepidocrocite, magnetite and maghemite are the main secondary iron minerals that have been detected by XAS analysis[36,79,90–92] though ferrihydrite and goethite have also been reported.[36,79,92]

3. NZVI PASSIVATION PROCESSES UNDER ANOXIC AND OXIC CONDITIONS

In this section, we review the state of knowledge with regard to the mechanism of passivation of NZVI under both anoxic and oxic conditions. Under anoxic conditions, the reaction with water is expected to be of principal importance for the formation of passivating

layers on the NZVI surface though attention is also given to the impact of other major solution constituents (such as carbonate, sulfate and nitrate) that may be present. Under oxic conditions, the presence of oxygen is obviously the major differentiator to anoxic systems with O_2 potentially influencing the reaction pathway of Fe(II) resulting from NZVI corrosion. Consideration is also given to the impact of the nature of the NZVI particle on the oxic passivation process with bimetallic particles of major interest.

3.1. Anoxic Conditions

With respect to the anoxic reaction of NZVI with water, the identification of the primary reductive products (particularly $Fe(OH)_2$ and magnetite) and the definition of the reaction mechanism have been well addressed by Filip et al.[39] These investigators[39] used "NANOFER 25P" NZVI particles of ~60 nm in diameter and a specific surface area of ~36 m^2g^{-1} that were thermally synthesized from iron oxide powder in H_2. Aging studies were undertaken under strictly anoxic conditions at both 25 ^oC and 80 ^oC. ^{57}Fe Mossbauer spectroscopy indicated that approximately 70% of the Fe(0) was transformed to $Fe(OH)_2$ after ~3000 h of reaction at 25 ^oC with this mineral transforming relatively rapidly (after ~200 h) to magnetite (Fe_3O_4) at 80 ^oC (Figure 2). Interestingly, the results obtained by Filip et al.[39] were at odds with the results of earlier workers such as Reardon et al.[94] who concluded that magnetite was also formed at 25 ^oC. Filip et al.[39] investigated this discrepancy and showed that the nanosheets of $Fe(OH)_2$ formed in their study could be rapidly transformed to magnetite on exposure to air during analysis by XRD – the solid characterization method used by Reardon et al.[94]. Quantum chemical calculations indicated a two-step reaction mechanism involving two one electron transfer processes; the first, which involved the breakage of the H-O bond of water, can be described by the reaction (Eq.1):

$$Fe^0 + H_2O \rightarrow HFe^{I}OH \quad (1)$$

which represents the rate-limiting step, and the second by (Eq.2):

$$HFe^{I}OH + H_2O \rightarrow Fe^{II}(OH)_2 + H_2 \quad (2)$$

Filip et al. [39] note that the existence of the HFeOH molecule has previously been demonstrated (by Zhang et al.[95]) by argon matrix isolation FTIR spectroscopy.

The nature of the corrosion products formed on NZVI upon exposure to anoxic solutions has been investigated in a more recent study with Liu et al.[78] concluding that the major passivation byproducts formed after 72 h of reaction were wüstite ($Fe^{II}O$), goethite and akageneite (Figure 3). These products differ markedly from those reported by Filip et al.[39] and beg the question of whether air exposure during TEM, XRD and Raman analyses resulted in transformation of the passivation products formed under anoxic conditions. Pullin et al.[79] investigated the nature of the passivation byproducts formed on exposure of NZVI to Milli-Q water for periods of more than four weeks with the nature of the passivation byproducts investigated by XAS. Amorphous passivation products (assigned as ferrihydrite) were formed within one day of exposure with the concurrent formation of magnetite. Over periods of up to four weeks, maghemite was observed to form with this oxide transforming slowly to "meta-stable" lepidocrocite. Over longer periods (greater than four weeks), all NZVI transformed to goethite with this iron oxide considered to be the likely "final state"

In summary, the anoxic corrosion of NZVI by water is dependent upon various factors, such as reaction time and temperature, with the major corrosion products observed being wustite, goethite and magnetite. It should be recognized, however, that the intrusion of oxygen either through the aging process or during analysis may confound the results of

experiments undertaken under supposed anoxic conditions. As such, investigators should pay particular attention to the possibility of unintended NZVI passivation during studies under anoxic conditions.

3.2. Oxic Conditions

The nature of the oxidation products formed on exposure of nanometer-sized Fe(0) particles to oxygen has been of interest for many years in view of the widespread use of ultrafine magnetic particles in magnetic recording, ferrofluids and catalysis with the nature of the oxide phases formed on exposure of small iron particles to an oxygen-containing atmosphere investigated by a number of groups.[96] Linderoth et al.[96] found, using Mössbauer spectroscopy, that the oxide layer grows quickly initially then slows down with the oxide layer consisting of a mixture of Fe_3O_4 and γ-Fe_2O_3. The kinetics of oxide layer formation followed a logarithmic rate law in accord with the Caberra-Mott model of oxidation[97] with multistage steps including i) dissociative adsorption of O_2 at the metal surface, ii) oxidation of surface metal ions, iii) incorporation of metal ions into the oxide layer, iv) diffusion of metal ions in the oxide layer, and v) reaction of metal ions with oxygen ions with the diffusion of metal ions in the oxide layer considered to be rate limiting.[98]

In comparison with the logarithmic behavior of oxide layer growth revealed from studies of passivation of iron particles in air, investigations of the oxidation of Fe(0) surfaces in the presence of water vapour reveal that reactions at the iron surface/water interface are rate limiting with an initial lag in oxide layer formation followed by an exponential increase in growth of the oxide layer.[99–101] Investigation of the aging of iron nanoparticles in aqueous solution by Sarathy et al.[102] revealed similar behavior with Fe(0) nanoparticles from Toda (RNIP-10DS) becoming more reactive (as determined by the rate of carbon tetrachloride (CCl_4) reduction) between 0 and ~2 days after exposure to water then gradually losing

reactivity over the ensuing 100 days. These changes in reactivity were correlated with evidence for destruction of an Fe(III) oxide film that initially covered the Fe(0) nanoparticles with subsequent formation of a new passivating mixed valence Fe(II)-Fe(III) oxide shell.[102]

Using quartz crystal microbalance measurements to quantify the rate of oxide layer formation, Greenlee et al.[103] showed similar behavior to that observed by Sarathy et al.[102] with an initial lag in oxide layer formation following by an exponential increase in mass of this layer (Region 1 in Figure S2). Decrease in water content of the solutions used (by replacing water with ethanol) resulted in an increase in the lag period before oxidation commenced and a decrease in the rate once oxidation had begun with these results confirming the critical role of H_2O in destabilizing the passivating layer initially present. As shown in Figure S2, this exponential increase in oxide layer growth was followed by a logarithmic decline in rate of corrosion at later times (Region 2) with this behavior in accord with the Caberra-Mott model described above. Greenlee et al.[103] showed that NZVI oxidized primarily to lepidocrocite with both carboxymethylcellulose (CMC) stabilizer and Ni slowing down the onset and extent of NZVI oxidation. Dong et al. [104–106] also showed that CMC and Ni slowed the aging of NZVI with the major products of oxidation found to be magnetite and maghemite.

Recent studies of NZVI-mediated oxidation by He et al.[36] confirmed the results of earlier studies by Joo et al.[30] that both Fe(II) and H_2O_2 are generated following 1 h exposure of NZVI to oxygenated water at circumneutral pH. The solid Fe species resulting from exposure of NZVI to oxygen were examined, as a function of exposure time, by EXAFS spectroscopy.[36] Linear combination fitting of the EXAFS results indicated that NZVI transformed to lepidocrocite via an intermediate ferrihydrite phase following exposure of NZVI to oxygenated water with essentially all NZVI transformed to ferric oxyhydroxides after two hours of exposure to the oxic aqueous environment (Figure 1d).[36]

In summary, crystalline iron (oxyhydr)oxides such as lepidocrocite, maghemite and magnetite appear to be the major products formed upon the oxic corrosion of NZVI. Ferrihydrite may form initially but Fe(II)-catalyzed transformation to more crystalline forms is likely to occur as a result of the high concentrations of surface-associated Fe(II) present. The particular iron (oxyhydr)oxide formed is likely to be a function of the molar ratio of Fe(II) to Fe(III) surface sites present with the relatively short lifetime of Fe(II) in these oxic systems also influencing the extent of crystallization.

4. FACTORS INFLUENCING NZVI PASSIVATION

Most of the published literature to date has addressed the impact of synthesis methods[107] and both organic and inorganic compounds[4,33,80,108–117] on the reactivity of NZVI with respect to target contaminants in the context of groundwater or wastewater remediation. In these studies, variations in the kinetic rate constants or extents of degradation were used as a means of assessing reactivity changes upon exposure to different cations or anions. However, very few attempts have been made to determine the corrosion mechanism(s) and to relate reactivity changes to the nature of the passivation byproducts formed[107] and the surfaces exposed to co-occurring solutes.[33,80]

4.1. Effect of Synthesis Methods

The elemental composition of NZVI can vary depending on the synthesis method used,[117,118] which may influence NZVI reactivity as well as the nature of the passivation byproducts. In most cases, Fe reduction is mediated by $NaBH_4$ ($NZVI^{BH}$) or H_2 ($NZVI^{H2}$) (Table 1). The XPS results revealed that the $NZVI^{H2}$ surfaces composed of Fe (37.9–50.9%), O (44.2–52.9%), B (0%), Na (0.7–8.1%) and S (0.9–1.9%, possibly from the $FeSO_4$ precursor).[107] The surface of the $NZVI^{BH}$ particles contained less Fe (20.0%–30.8%) and S

(0.0%–0.5%), but greater O (49.1–59.2%), B (12.0–16.0%) and Na (0.5–14.5%).[107,118] Moreover, it was found that the S on the $NZVI^{BH}$ surface was in an oxidized form, whereas the S present on the surface of the $NZVI^{H2}$ particles was in reduced form.[107] Interestingly, $NZVI^{H2}$ exhibited lower reactivity than $NZVI^{BH}$ for the transformation of CCl_4 to chloroform ($CHCl_3$), presumably due to the high Fe/O ratio (possibly associated with the presence of a magnetite shell) on the $NZVI^{H2}$ surfaces.[107] This hypothesis was supported by the low ability of nanoscale magnetite to transform CCl_4.[119] These results serve to demonstrate that synthesis methods could alter the surface reactivity of NZVI and potentially its passivation mechanism.

As noted above, the use of $NaBH_4$ during the synthesis of $NZVI^{BH}$ can result in the occurrence of B on the surface of $NZVI^{BH}$ [120]. Recently, it has been reported that $NaBH_4$ can induce the disintegration of $NZVI^{BH}$ particles, resulting in the formation of significantly smaller particles.[121] This phenomenon may be induced by chemical etching of the passivated NZVI surface (coated, for example, by iron oxides such as magnetite) with this result consistent with the ability of $NaBH_4$ to induce the disintegration of microscale magnetite into nanoscale magnetite.[122] Although these authors did not compare their results to $NZVI^{H2}$, the disparity in elemental surface composition (e.g., more Fe and S with less Na on the $NZVI^{H2}$ surfaces) may possibly cause reactions to proceed differently.

4.2. Effect of Inorganic Compounds

Although the corrosion rate of NZVI and the nature of the passivation byproducts can be significantly affected by the presence of anionic or cationic inorganic species, very few studies have focused on this topic.[33,80] The corrosion phenomenon is dependent on several factors including the type and concentration of aqueous species, reaction time and oxic/anoxic environments.[33,80] It has been reported that the presence of common groundwater anions may promote or inhibit the corrosion of NZVI, however limited insight into the mechanism(s) of

the effects of anions is available.[33,80] After six months of aging in pH unbuffered and anoxic solutions containing 10 mM of either HCO_3^-, SO_4^{2-}, NO_3^-, HPO_4^{2-} or Cl^-, NZVI (commercial sample, RNIP 10-DP) was found to predominantly transform to vivianite in the phosphate-aged sample and schwertmannite in the sulfate-aged sample (Figure S3).[33] Both the fresh NZVI and the sample aged for six months in 10 mM nitrate predominantly contained Fe(0) and magnetite.[33] The pH of the suspensions containing the different anions ranged from 9.0–11.8, indicating that the observed transformations occurred under alkaline conditions.[33] Using the same concentrations of the anionic species, $NZVI^{H2}$ particles have also been found to undergo corrosion into different iron phases after 16 weeks.[80] For example, HCO_3^- produced goethite , NO_3^- resulted in the formation of magnetite/maghemite and SO_4^{2-} and Cl^- produced a mixture of magnetite/maghemite, lepidocrocite and goethite (Figure S4).[80] It was observed that the corrosion rate of NZVI increased in the order $HCO_3^- > Cl^-/SO_4^{2-} > NO_3^-$, however pH was only measured in experiments in which the uptake of Cu and Zn by the corroded NZVI was examined over a time period of 4 weeks.[80] As such, the influence of this critical parameter on the nature of the formed passivation byproducts is unknown. Elsewhere, Kim et al.[117] have reported that a commercial NZVI (NANOFER 25DS) coated by S-based inorganic compounds was oxidized to magnetite in a synthetic groundwater containing Cl^- (1.95 mN), HCO_3^- (1.14 mN), NO_3^- (0.15 mN) and SO_4^{2-} (0.44 mM). In contrast, iron carbonate hydroxide hydrate was detected as a major passivation byproduct in the presence of humic acid (2.5 mg L^{-1}).

Xie and Cwiertny[4] have reported that the presence of Cl^-, SO_4^{2-} and ClO_4^- almost completely inhibited the reduction of 1,1,1,2-tetrachloroethane by NZVI over a time period of one month, irrespective of the nature or concentration of the anion present or pH. In contrast, the longevity toward degrading this contaminant was dependent upon the concentrations of NO_3^- and HCO_3^- with complete reactivity loss over 1 d and 14 d, respectively, in 25 mM

suspensions. In addition, XRD analyses suggested that the loss in reactivity in NO_3^- suspensions resulted from Fe(0) conversion into magnetite, whereas the formation of iron carbonate hydroxide limited reactivity in the HCO_3^- suspensions (Figure 4). Furthermore, Liu et al.[108] reported that trichloroethylene (TCE) reduction rates by NZVI are highly dependent on anion concentrations. For example, concentrations below 1 mM NO_3^- slightly increased the reduction rate but the reaction was retarded at NO_3^- concentrations between 1 and 3 mM and ceased at 5 mM. It was speculated that high NO_3^- concentrations may shift the TCE reduction reaction from one of cathodic control (i.e., the reduction of TCE) to anodic control (i.e., the release of Fe^{2+} and electrons) resulting in significant surface passivation.

On the other hand, Su et al.[109] reported that the rate of degradation of hexachlorobenzene by NZVI was not influenced by the presence of HCO_3^-, Mg^{2+} or Na^+ (over the concentration range of 0.8–7.7 mM). However, the rate of degradation was enhanced in the presence of 7.7 mM Cl^- or SO_4^{2-} due to the promotion of corrosion but inhibited in the presence of 7.7 mM of NO_3^- due to the competition between the anions and contaminants for reactive surface sites. However, it has been observed that the addition of Na_2SO_4 inhibited the degradation of pentachlorophenol (PCP) by Pd/Fe bimetallic nanoparticles in the range of 2.5–10 mM[110] and the decolorization of methyl orange by NZVI particles at 14 mM.[111] Researchers generally attribute the inhibitory effects of common groundwater anions to their affinity for surface sites on the iron (oxyhydr)oxides coating the NZVI with the resulting surface complexes limiting the ability of contaminants to associate with the surface. Consistently, the inhibition effect has been found to increase in the order of $Cl^- < SO_4^{2-} < HPO_4^2$ for nitrate reduction by Peerless Fe(0)[112] and $Cl^- < SO_4^{2-} < HCO_3^- < HPO_4^{2-}$ for TCE reduction by NZVI.[108]

Given that the standard reduction potential of Na^+ ions (−2.71 V) is below that of Fe^{2+} ions (−0.44 V), Na^+ ions do not affect degradation reactions mediated by Fe(0).[109] However, Cu^{2+} (0.8–7.7 mM) has been shown to enhance the degradation kinetics of hexachlorobenzene

by NZVI whereas Fe^{2+} (0.8–7.7 mM) has been reported to inhibit the degradation reaction due to the formation of passivation layers on the particle surfaces.[109] Moreover, Cu^{2+} (5–10 mM), Ni^{2+} (5–10 mM) and Fe^{3+} (1.67–5 mM) have been observed to enhance PCP degradation by Pd/Fe nanoparticles due to the deposition of reduced copper and nickel species on the Fe surfaces.[110] The standard reduction potentials of the Cu^{2+} (+0.34 V) and Ni^{2+} (−0.257 V) cations are significantly higher than that of Fe^{2+} (−0.44 V) and, as such, the reduction of Cu^{2+} or Ni^{2+} ions to their elemental forms is thermodynamically favorable.[113,114] In the case of the Fe^{3+} cation, the enhancement observed in the PCP degradation was attributed to a decrease of pH resulting from the addition of the iron salt.[110] Furthermore, spectroscopic investigations of the structural evolution of NZVI in anoxic Co^{2+} solutions revealed that Co^{2+} was heterogeneously reduced (E_0 = − 0.28 V) and migrated to the NZVI core leading to its continuous removal from the solution.[115] However, information on whether Co^{2+} affects the nature of passivation byproducts is lacking though dissolution of sheet or shell structures upon metal complexation on the Fe surface has been reported in depassivation studies of micro-scale ZVI (~70 mesh) by Liu et al. (Figure 5).[85,116]

In summary, anionic ligands such as phosphate, silicate and sulfate may be readily adsorbed onto iron corrosion products, affecting the reactivity of NZVI particles. Hard cations (such as Ca^{2+} and Mg^{2+}) and transition cationic metals (such as Ni^{2+}, Cu^{2+} and Co^{2+}) may exhibit promotive or inhibitive effects depending on their properties. However, the main secondary iron minerals formed during the reduction reaction have rarely been identified.

4.3. Effect of Organic Compounds

The use of organic ligands in NZVI studies has been investigated in the context of colloidal stabilization to increase particle mobility and improve redox reactivity. For example, chemical stabilizers (such as humic acid, polyacrylic acid and anionic or nonionic surfactants)

498 have been used to increase electrostatic repulsion effects and the stability of NZVI
499 particles.[16,20,123,124] However, minimal attention has been given to the impact of stabilizers on
500 the passivation of NZVI.

501 In oxygenated solutions, NZVI can undergo four electron transfer steps leading to the
502 formation of reactive species such as HO^* and Fe(IV), which can potentially be utilized in the
503 oxidative degradation of certain organic contaminants. The addition of iron-chelating agents
504 such as oxalate, nitrilotriacetic acid, ethylenediaminetetraacetic acid, tetrapolyphosphate and
505 polyoxometalate may accelerate the formation of ROS by mediating electron transfer from
506 NZVI to oxygen (e.g., changing the four-electron transfer process to a two-electron transfer
507 process) and by forming soluble complexes with iron at neutral pH values.[125–127] Although
508 these studies did not assess the NZVI passivation byproducts in the presence of iron
509 complexing agents and O_2, the acceleration of the NZVI corrosion rate is expected under such
510 conditions.

511 The effects of short chain organic acids (e.g., formic, oxalic and citric acid) on nitrate
512 reduction by Fe(0) has been observed to increase in accordance with the degree to which the
513 ligands adsorb to the surface of iron (oxyhydr)oxides or the stability constants of the aqueous
514 complexes between Fe(III) and the organic ligands.[112] The blockage of reactive sites on the
515 surface of Fe(0) and its passivation byproducts by the adsorption of ligands through an inner-
516 sphere complexation mechanism may be responsible for the observed decrease in reduction
517 rate. Unfortunately, information on whether and/or how the specific adsorption of ligands to
518 the outer layers of corrosion products may alter the ongoing passivation or structural
519 evolution of NZVI is very scarce.

520

521 **5. DEPASSIVATION STRATEGIES**

As discussed in the previous sections, most NZVI studies have focused on the passivation of NZVI after its use in water decontamination reactions. A decrease in NZVI reactivity is considered one of the major issues and a solution is required if NZVI is to be used to effectively degrade contaminants. In this section, a variety of depassivation strategies (including physical, chemical and biological approaches) are introduced to enhance and/or prolong the reactivity of NZVI. Particular attention is given to the use of depassivation strategies before, during and after the decontamination process.

5.1. Depassivation before decontamination

A well-known limitation to the broad application of NZVI for contaminant degradation is rapid pyrophoric reaction in air and surface passivation in aqueous solutions. This has led to studies examining possible synthesis procedures that can be used to produce reactive NZVI, i.e., NZVI that is atmospherically stable[86] or stable in aqueous phase.[128] For example, the shell-modified NZVI particles produced by Kim et al.[86] after controlled air-oxidation at various flow rates for 1 d did not ignite upon later exposure to atmospheric conditions. Shorter and longer controlled oxidation times resulted in spontaneous combustion or significantly decreased TCE degradation rates, respectively.[86] The optimal shell-modified NZVI particles exhibited a TCE degradation rate that was 78% of that obtained for fresh NZVI (Figure S5). It was also revealed that after aging in water for 1 d, both the fresh and shell-modified NZVI exhibited similar TCE degradation rate constants. It was conjectured that surface depassivation of the shell-modified particles was the cause for this observation, however, no mechanisms were examined or postulated.

It has been reported that annealing can induce structural and chemical changes in NZVI, with re-ordering and recrystallization of the inner Fe core, so as to eliminate defects and impurities.[129] In this case, the thickness of the surface oxide layer decreased from 3–4 nm to 2

547 nm by vacuum annealing at 500 °C with an accompanying change of the surface oxide from
548 magnetite to wüstite and the migration of boron and carbon to the particle surface.[129] This
549 depassivation process was postulated to improve the corrosion resistance and reactive lifespan
550 of NZVI for environmental applications. A subsequent study performed by this group
551 revealed that NZVI reactivity was significantly enhanced (by a factor of 30), with respect to
552 the degradation of TCE and cis-1,2-dichloroethene, when compared to that of fresh NZVI due
553 to efficient electron transfer from Fe(0) to the contaminants.[130]

554 In recent years there has been an explosion of interest in the sulfidation of NZVI during
555 its synthesis to prevent surface passivation reactions that result from the reduction of water.
556 Using variations of the method first outlined by Kim et al.,[128] several studies have revealed
557 that sulfidated NZVI is superior to NZVI in decontamination reactions.[35,128,131] Enhanced
558 decontamination by sulfidated NZVI has been hypothesized to result from the inhibition of
559 corrosion in water.[65] The formation of nanocrystalline FeS phases on the surfaces of
560 sulfidated NZVI, resulting in a high surface area and good electrical conductivity, has been
561 suggested to be responsible for the high reactivity of these nanoparticles toward contaminants
562 (Figure S6).[128] From a molecular point of view, dechlorination by reductive elimination may
563 be favored over hydrogenolysis as a result of sulfidation.[65] In addition, the surface of
564 sulfidated NZVI may act as a more efficient conductor of electrons from the inner Fe(0) to the
565 surface layers than iron (oxyhydr)oxides.[131,132] Two recent review papers have highlighted
566 progress made in this research area.[65,133]

567

568 **5.2. Depassivation during/after decontamination**

569 A significant amount of effort has been expended on the investigation of methods to
570 extend the longevity of NZVI during the removal of environmental contaminants. For
571 example, Bae and Lee[8] recently demonstrated that an endogenous electron shuttle (i.e.,

572 riboflavin) can enhance the long-term dechlorination of CCl_4 by NZVI. Results from TEM
573 surface analyses revealed the removal of the passivated layer (Figure S7), presumably due to
574 reductive dissolution by riboflavin, which could result in an increase in the rate of electron
575 transfer. In addition, Wang et al.[14] revealed that the addition of humic acid enhanced the rate
576 and extent of 4-chlorobiphenyl degradation by NZVI, given that the humic acid acted as an
577 electron shuttle, thus leading to the rapid transfer of electrons from NZVI to the contaminant.
578 Although the investigators did not investigate the depassivation of NZVI,[8,14] their
579 experimental results indicated that other electron shuttles such as quinone moieties (e.g., *p*-
580 hydroquinone, lawsone, 9,10-anthraquinone-2,6-disulfonate (AQDS), etc.) may also lead to
581 an increase in the longevity of NZVI.

582 Ultrasound has commonly been used to improve the dispersivity and stability of NZVI
583 during decontamination of wastewater.[134,135] This process induces cavitation leading to
584 extremely high local temperatures (up to 10000 K) and pressures (up to 5000 bar).[136] This can
585 cause pitting and cracking at particle surfaces resulting in the removal of the passivated
586 surface (oxyhydr)oxide layer.[137] The enhanced removal of several elements, including Zn^{2+},
587 Pb^{2+} and Cu^{2+} has been observed following the application of ultrasound with the increased
588 removal due probably to the removal of the passivated layer. [136]

589 There have been very few studies on the regeneration of passivated NZVI after
590 decontamination[138] although several studies have been conducted on ZVI.[85,116,139] Due to the
591 different Fe (oxyhydr)oxides that may form on corrosion of NZVI and ZVI and the inherent
592 physical and chemical differences of these particles, it is not appropriate to necessarily
593 assume similar mechanistic processes are operative for ZVI and NZVI. For example, a
594 significant enhancement of TCE reduction was observed when an iron reducing bacteria
595 (*Shewanella putrefaciens*) was inoculated into a passivated ZVI suspension but not when
596 introduced to NZVI.[138] It was speculated that the biologically-mediated reductive dissolution

of the passivating layer re-exposed the ZVI Fe(0) core whereas a minimal amount of Fe(0) was conserved in the case of passivated NZVI. Overall, the lack of studies on NZVI depassivation after decontamination reactions is a result of the small size and highly reactive nature of NZVI, which generally leads to its rapid transformation to Fe(II) and Fe(III) minerals.

6. ENVIRONMENTAL SIGNIFICANCE AND FUTURE APPLICATIONS

NZVI has been one of the most intensively studied nanomaterials in environmental engineering over the past 20 years, particularly in relation to its potential use in remediating soil, groundwater and wastewater. Despite the extensive *in situ* and *ex-situ* use of NZVI for contaminant removal, rapid surface passivation resulting in loss of NZVI reactivity is considered one of the most severe problems with regard to its effective application. As discussed in this review, the nature and extent of NZVI passivation may differ markedly depending on the particular conditions in which NZVI is applied (Figure 6). As such, the need exists to investigate the particular passivation mechanism, the factors that influence the rate and extent of passivation and possible depassivation techniques suited to promoting the efficacy of NZVI for each proposed application.

Most of the published literature to date has investigated the reactivity of NZVI with very little attention paid to its passivation mechanisms. The reaction between NZVI and contaminants is generally used to assess particle reactivity, however analyses of NZVI transformations have rarely been conducted by investigators. Moreover, passivation effects are more significant when NZVI is applied at a pilot- and/or field-scale due to the presence of many influencing factors (e.g., long reaction time, O_2 levels, presence of inorganic and organic contaminants and biotic influences). A systematic analysis of the effects of

passivation is therefore necessary to provide a comprehensive understanding of NZVI chemistry during long-term applications (e.g., groundwater and soil remediation).

In this review, the most recent information with respect to the characterization techniques for identifying passivation mechanisms have been summarized, in addition to important factors that influence depassivation under different O_2 conditions and thereby extend the longevity of NZVI. It becomes clear that there are significant challenges to overcome to further advance NZVI as a remedial agent for environmental pollution. These challenges include: (i) the establishment of advanced time-resolved methodologies to monitor NZVI transformations; (ii) the evaluation of the contribution of passivation byproducts to sequential contaminant removal; (iii) the investigation of microbial populations promoted by the passivation byproducts after soil and groundwater remediation and (iv) the development of novel and efficient depassivation strategies during and after NZVI application.

In engineered systems (such as wastewater treatment), the assessment of NZVI corrosion byproducts and depassivation ways in order to improve and/or maintain contaminant removal performance will be critical for developing a cost-effective NZVI-based technologies and designing large-scale applications. In natural systems (such as soil and groundwater environments) where nanoparticles are injected into affected zones, a comprehensive examination of the transformation and mobility of the injected nanoparticles is essential for ecological risk assessments. This will improve our ability to develop new simulation tools for accurately predicting the overall performance of NZVI-based technologies as well as the fate of NZVI particles in natural systems.

ASSOCIATED CONTENT

Supporting Information

The Supporting Information is available free of charge via on the ACS publications websites at DOI:

Figures S1 to S7 (PDF).

ACKNOWLEDGMENTS

This research was partially supported by the framework of International Cooperation Program managed by National Research Foundation of Korea (NRF-2017K1A3A1A21013653) and Campus France (PHC STAR).

REFERENCES

(1) Alowitz, M. J.; Scherer, M. M., Kinetics of nitrate, nitrite, and Cr(VI) reduction by iron metal. *Environ. Sci. Technol.* **2002,** *36* (3), 299–306.

(2) Phillips, D. H.; Van Nooten, T.; Bastiaens, L.; Russell, M. I.; Dickson, K.; Plant, S.; Ahad, J. M. E.; Newton, T.; Elliot, T.; Kalin, R. M. Ten year performance evaluation of a field–scale zero–valent iron permeable reactive barrier installed to remediate trichloroethene contaminated groundwater. *Environ. Sci. Technol.* **2010,** *44* (10), 3861–3869.

(3) Bae, S.; Lee, W., Inhibition of nZVI reactivity by magnetite during the reductive degradation of 1,1,1–TCA in nZVI/magnetite suspension. *Appl. Catal. B–Environ.* **2010,** *96* (1–2), 10–17.

(4) Xie, Y.; Cwiertny, D. M., Influence of anionic cosolutes and pH on nanoscale zerovalent iron longevity: time scales and mechanisms of reactivity loss toward 1,1,1,2-tetrachloroethane and Cr(VI). *Environ. Sci. Technol.* **2012,** *46* (15), 8365–8373.

(5) Lowry, G. V.; Johnson, K. M., Congener-specific dechlorination of dissolved PCBs by microscale and nanoscale zerovalent iron in a water/methanol solution. *Environ. Sci. Technol.* **2004,** *38* (19), 5208–5216.

(6) Bae, S.; Hanna, K., Reactivity of nanoscale zero-valent iron in unbuffered systems: effect of pH and Fe(II) dissolution. *Environ. Sci. Technol.* **2015,** *49* (17), 10536–10543.

(7) Smith, K. S.; Huyck, H. L. O. An overview of the abundance, relative mobility, bioavailability, and human toxicity of metals. In *The Environmental Geochemistry of Mineral Deposits. Part A: Processes, Techniques, and Health Issues*; Plumlee, G. S.; Logsdon, M. J., Eds.; Society of Economic Geologists: Littleton, CO, **1999**; Vol. 6A.

(8) Bae, S.; Lee, W., Influence of riboflavin on nanoscale zero–valent iron reactivity during the degradation of carbon tetrachloride. *Environ. Sci. Technol.* **2014,** *48* (4), 2368–2376.

(9) Song, H.; Carraway, E. R. Reduction of chlorinated ethanes by nanosized zero-valent iron: kinetics, pathways, and effects of reaction conditions. *Environ. Sci. Technol*. **2005**, 39, 6237–6245.

(10) Wang, C. B.; Zhang, W. X. Synthesizing nanoscale iron particles for rapid and complete dechlorination of TCE and PCBs. *Environ. Sci. Technol*. **1997**, 31, 2154–2156.

(11) Cheng, R.; Wang, J. L.; Zhang, W. X. Comparison of reductive dechlorination of p-chlorophenol using Fe^0 and nanosized Fe^0. *J. Hazard. Mater.* **2007,** *144* (1–2), 334–339.

(12) Ryu, A.; Jeong, S. W.; Jang, A.; Choi, H., Reduction of highly concentrated nitrate using nanoscale zero-valent iron: Effects of aggregation and catalyst on reactivity. *Appl. Catal. B–Environ.* **2011,** *105* (1–2), 128–135.

(13) Shih, Y. H.; Hsu, C. Y.; Su, Y. F. Reduction of hexachlorobenzene by nanoscale zero-valent iron: Kinetics, pH effect, and degradation mechanism. *Sep. Purif. Tech.* **2011,** *76* (3), 268–274.

(14) Wang, Y.; Zhou, D. M.; Wang, Y. J.; Zhu, X. D.; Jin, S. Y. Humic acid and metal ions accelerating the dechlorination of 4-chlorobiphenyl by nanoscale zero–valent iron. *J. Environ. Sci–China* **2011,** *23* (8), 1286–1292.

(15) Chekli, L.; Bayatsarmadi, B.; Sekine, R.; Sarkar, B.; Shen, A. M.; Scheckel, K. G.; Skinner, W.; Naidu, R.; Shon, H. K.; Lombi, E.; Donner, E. Analytical characterisation of nanoscale zero-valent iron: A methodological review. *Anal. Chim. Acta* **2016,** *903*, 13–35.

(16) Giasuddin, A. B. M.; Kanel, S. R.; Choi, H. Adsorption of humic acid onto nanoscale zerovalent iron and its effect on arsenic removal. *Environ. Sci. Technol.* **2007,** *41* (6), 2022–2027.

(17) Li, X. Q.; Cao, J. S.; Zhang, W. X. Stoichiometry of Cr(VI) immobilization using nanoscale zerovalent iron (nZVI): A study with high-resolution X-ray photoelectron spectroscopy (HR-XPS). *Ind. Eng. Chem. Res.* **2008,** *47* (7), 2131–2139.
(18) Dong, H. R.; Guan, X. H.; Lo, I. M. C. Fate of As(V)-treated nano zero–valent iron: Determination of arsenic desorption potential under varying environmental conditions by phosphate extraction. *Water Res.* **2012,** *46* (13), 4071–4080.
(19) Kanel, S. R.; Greneche, J. M.; Choi, H. Arsenic(V) removal from groundwater using nano scale zero-valent iron as a colloidal reactive barrier material. *Environ. Sci. Technol.* **2006,** *40* (6), 2045–2050.
(20) Kanel, S. R.; Nepal, D.; Manning, B.; Choi, H. Transport of surface-modified iron nanoparticle in porous media and application to arsenic(III) remediation. *J. Nanopart. Res.* **2007,** *9* (5), 725–735.
(21) Yan, W.; Vasic, R.; Frenkel, A. I.; Koel, B. E. Intraparticle reduction of arsenite (As(III)) by nanoscale zerovalent iron (nZVI) investigated with in situ X-ray absorption spectroscopy. *Environ. Sci. Technol.* **2012,** *46* (13), 7018–7026.
(22) Kanel, S. R.; Manning, B.; Charlet, L.; Choi, H. Removal of arsenic(III) from groundwater by nanoscale zero-valent iron. *Environ. Sci. Technol.* **2005,** *39* (5), 1291–1298.
(23) Zhang, Y. L.; Li, Y. T.; Dai, C. M.; Zhou, X. F.; Zhang, W. X. Sequestration of Cd(II) with nanoscale zero-valent iron (nZVI): Characterization and test in a two-stage system. *Chem. Eng. J.* **2014,** *244*, 218–226.
(24) Tsarev, S.; Collins, R. N.; Ilton, E. S.; Fahy, A.; Waite, T. D. The short-term reduction of uranium by nanoscale zero-valent iron (nZVI): role of oxide shell, reduction mechanism and the formation of U(V)-carbonate phases. *Environ. Sci. Nano* 2017, 4 (6), 1304–1313.
(25) Sihn, Y.; Bae, S.; Lee, W. Formation of surface mediated iron colloids during U(VI) and nZVI interaction, *Adv. Environ. Res.* **2013**, *2*, 167–177.
(26) Sheng, G. D.; Shao, X. Y.; Li, Y. M.; Li, J. F.; Dong, H. P.; Cheng, W.; Gao, X.; Huang, Y. Y. Enhanced removal of uranium(VI) by nanoscale zerovalent iron supported on Na-bentonite and an investigation of mechanism. *J. Phys. Chem. A* **2014,** *118 (16)*, 2952–2958.
(27) Fan, D. M.; Anitori, R. P.; Tebo, B. M.; Tratnyek, P. G.; Pacheco, J. S. L.; Kukkadapu, R. K.; Engelhard, M. H.; Bowden, M. E.; Kovarik, L.; Arey, B. W. Reductive sequestration of pertechnetate ($^{99}TcO_4^-$) by nano zerovalent iron (nZVI) transformed by abiotic sulfide. *Environ. Sci. Technol.* **2013,** *47* (10), 5302–5310.
(28) Machado, S.; Stawinski, W.; Slonina, P.; Pinto, A. R.; Grosso, J. P.; Nouws, H. P. A.; Albergaria, J. T.; Delerue-Matos, C. Application of green zero-valent iron nanoparticles to the remediation of soils contaminated with ibuprofen. *Sci. Total. Environ.* **2013,** *461*, 323–329.
(29) Karim, S.; Bae, S.; Greenwood, D.; Hanna, K.; Singhal, N. Degradation of 17 alpha-ethinylestradiol by nano zero valent iron under different pH and dissolved oxygen levels. *Water Res.* **2017,** *125*, 32–41.
(30) Joo, S. H.; Feitz, A. J.; Waite, T. D. Oxidative degradation of the carbothioate herbicide, molinate, using nanoscale zero–valent iron. *Environ. Sci. Technol.* **2004,** *38 (7)*, 2242–2247.
(31) Feitz, A. J.; Joo, S. H.; Guan, J.; Sun, Q.; Sedlak, D. L.; Waite, T. D. Oxidative transformation of contaminants using colloidal zero-valent iron. *Colloids Surf., A* **2005,** *265 (1–3)*, 88–94.

(32) Phenrat, T.; Saleh, N.; Sirk, K.; Tilton, R. D.; Lowry, G. V. Aggregation and sedimentation of aqueous nanoscale zerovalent iron dispersions. *Environ. Sci. Technol.* **2007,** *41* (1), 284–290.
(33) Reinsch, B. C.; Forsberg, B.; Penn, R. L.; Kim, C. S.; Lowry, G. V. Chemical transformations during aging of zerovalent iron nanoparticles in the presence of common groundwater dissolved constituents. *Environ. Sci. Technol.* **2010,** *44* (9), 3455–3461.
(34) Wang, F. F.; Wu, Y.; Gao, Y.; Li, H.; Chen, Z. L. Effect of humic acid, oxalate and phosphate on Fenton–like oxidation of microcystin-LR by nanoscale zero-valent iron. *Sep. Purif. Tech.* **2016,** *170*, 337–343.
(35) Fan, D. M.; Johnson, G. O.; Tratnyek, P. G.; Johnson, R. L. Sulfidation of nano zerovalent iron (nZVI) for improved selectivity during in–situ chemical reduction (ISCR). *Environ. Sci. Technol.* **2016,** *50* (17), 9558–9565.
(36) He, D.; Ma, J. X.; Collins, R. N.; Waite, T. D. Effect of structural transformation of nanoparticulate zero-valent iron on generation of reactive oxygen species. *Environ. Sci. Technol.* **2016,** *50* (7), 3820–3828.
(37) Ahn, J.; Kim, C.; Kim, H.; Hwang, K.; Hwang, I. Effects of oxidants on in situ treatment of a DNAPL source by nanoscale zero-valent iron: A field study. *Water Res.* **2016**, *107*, 57–65.
(38) Liu, A. R.; Liu, J.; Pan, B. C.; Zhang, W. X. Formation of lepidocrocite (gamma–FeOOH) from oxidation of nanoscale zero-valent iron (nZVI) in oxygenated water. *RSC Adv.* **2014,** *4* (101), 57377–57382.
(39) Filip, J.; Karlicky, F.; Marusak, Z.; Lazar, P.; Cernik, M.; Otyepka, M.; Zboril, R. Anaerobic reaction of nanoscale zerovalent iron with water: Mechanism and kinetics. *J. Phys. Chem. C* **2014,** *118* (25), 13817–13825.
(40) Jung, Y.; Choi, J.; Lee, W., Spectroscopic investigation of magnetite surface for the reduction of hexavalent chromium. *Chemosphere* **2007,** *68* (10), 1968–1975.
(41) Rashid, M.; Price, N. T.; Pinilla, M. A. G.; O'Shea, K. E. Effective removal of phosphate from aqueous solution using humic acid coated magnetite nanoparticles. *Water Res.* **2017,** *123*, 353–360.
(42) Bharath, G.; Alhseinat, E.; Ponpandian, N.; Khan, M. A.; Siddiqui, M. R.; Ahmed, F.; Alsharaeh, E. H. Development of adsorption and electrosorption techniques for removal of organic and inorganic pollutants from wastewater using novel magnetite/porous graphene-based nanocomposites. *Sep. Purif. Technol.* **2017,** *188*, 206–218.
(43) Shi, J.; Li, H. Y.; Lu, H. G.; Zhao, X. W. Use of carboxyl functional magnetite nanoparticles as potential sorbents for the removal of heavy metal ions from aqueous solution. *J. Chem. Eng. Data* **2015,** *60 (7)*, 2035–2041.
(44) Bae, S.; Joo, J. B.; Lee, W. Reductive dechlorination of carbon tetrachloride by bioreduction of nontronite. *J. Hazard. Mater.* **2017,** *334*, 104–111.
(45) Jeon, K.; Lee, N.; Bae, S.; Goddard, W. A.; Kim, H.; Lee, W. Theoretical and experimental studies of the dechlorination mechanism of carbon tetrachloride on a vivianite ferrous phosphate surface. *J. Phys. Chem. A* **2015,** *119 (22)*, 5714–5722.
(46) Bae, S.; Lee, W. Enhanced reductive degradation of carbon tetrachloride by biogenic vivianite and Fe(II). *Geochim. Cosmochim. Acta* **2012,** *85*, 170–186.
(47) Veeramani, H.; Alessi, D. S.; Suvorova, E. I.; Lezama-Pacheco, J. S.; Stubbs, J. E.; Sharp, J. O.; Dippon, U.; Kappler, A.; Bargar, J. R.; Bernier-Latmani, R. Products of abiotic U(VI) reduction by biogenic magnetite and vivianite. *Geochim. Cosmochim. Acta* **2011,** *75 (9)*, 2512–2528.

795 (48) Etique, M.; Zegeye, A.; Gregoire, B.; Carteret, C.; Ruby, C. Nitrate reduction by mixed
796 iron(II-III) hydroxycarbonate green rust in the presence of phosphate anions: The key
797 parameters influencing the ammonium selectivity. *Water Res.* **2014,** *62*, 29–39.
798 (49) Guerbois, D.; Ona–Nguema, G.; Morin, G.; Abdelmoula, M.; Laverman, A. M.; Mouchel,
799 J. M.; Barthelemy, K.; Maillot, F.; Brest, J. Nitrite reduction by biogenic
800 hydroxycarbonate green rusts: Evidence for hydroxy-nitrite green rust formation as an
801 intermediate reaction product. *Environ. Sci. Technol.* **2014,** *48 (8)*, 4505–4514.
802 (50) Lee, W.; Batchelor, B. Abiotic, reductive dechlorination of chlorinated ethylenes by iron-
803 bearing soil minerals. 2. Green rust. *Environ. Sci. Technol.* **2002,** *36 (24)*, 5348–5354.
804 (51) Orsetti, S.; Laskov, C.; Haderlein, S. B., Electron transfer between iron minerals and
805 quinones: Estimating the reduction potential of the Fe(II)-goethite surface from AQDS
806 speciation. *Environ. Sci. Technol.* **2013,** *47 (24)*, 14161–14168.
807 (52) Pecher, K.; Haderlein, S. B.; Schwarzenbach, R. P. Reduction of polyhalogenated
808 methanes by surface-bound Fe(II) in aqueous suspensions of iron oxides. *Environ. Sci.*
809 *Technol.* **2002,** *36 (8)*, 1734–1741.
810 (53) Jiang, W. J.; Pelaez, M.; Dionysiou, D. D.; Entezari, M. H.; Tsoutsou, D.; O'Shea, K.
811 Chromium(VI) removal by maghemite nanoparticles. *Chem. Eng. J.* **2013,** *222*, 527–533.
812 (54) Liu, H. B.; Chen, T. H.; Frost, R. L. An overview of the role of goethite surfaces in the
813 environment. *Chemosphere* **2014,** *103*, 1–11.
814 (55) Wang, S. S.; Gao, B.; Zimmerman, A. R.; Li, Y. C.; Ma, L.; Harris, W. G.; Migliaccio, K.
815 W. Removal of arsenic by magnetic biochar prepared from pinewood and natural
816 hematite. *Bioresour. Technol.* **2015,** *175*, 391–395.
817 (56) Zhang, Y.; Zhi, Y.; Liu, J.; Ghoshal, S. Sorption of perfluoroalkyl acids to fresh and aged
818 nanoscale zerovalent iron particles. *Environ. Sci. Tech.* **2018**, *52*, 6300–6308.
819 (57) Wang, S.; Gao, B.; Li, Y.; Creamer, A. E.; He, F. Adsorptive removal of arsenate from
820 aqueous solutions by biochar supported zero–valent iron nanocomposite: Batch and
821 continuous flow tests. *J. Hazard. Mater.* **2017**, *322*, 172–181
822 (58) Phenrat, T.; Long, T. C.; Lowry, G. V.; Veronesi, B. Partial oxidation ("aging") and
823 surface modification decrease the toxicity of nanosized zerovalent iron. *Environ. Sci.*
824 *Technol.* **2009,** *43 (1)*, 195–200.
825 (59) Auffan, M.; Achouak, W.; Rose, J.; Roncato, M. A.; Chaneac, C.; Waite, D. T.; Masion,
826 A.; Woicik, J. C.; Wiesner, M. R.; Bottero, J. Y. Relation between the redox state of iron-
827 based nanoparticles and their cytotoxicity toward Escherichia coli. *Environ. Sci. Technol.*
828 **2008,** *42 (17)*, 6730–6735.
829 (60) Yan, W. L.; Ramos, M. A. V.; Koel, B. E.; Zhang, W. X. As(III) sequestration by iron
830 nanoparticles: Study of solid-phase redox transformations with X-ray photoelectron
831 spectroscopy. *J. Phys. Chem. C* **2012**, *116 (9)*, 5303–5311.
832 (61) Johnson, R. L.; Nurmi, J. T.; O'Brien Johnson, G. S.; Fan, D.; O'Brien Johnson, R. L.;
833 Shi, Z.; Salter–Blanc, A. J.; Tratnyek, P. G.; Lowry, G. V. Field-scale transport and
834 transformation of carboxymethylcellulose-stabilized nano zero-valent iron. *Environ. Sci.*
835 *Technol.* **2013**, *47*, 1573−1580.
836 (62) Kocur, C. M.; Chowdhury, A. I.; Sakulchaicharoen, N.; Boparai, H. K.; Weber, K. P.;
837 Sharma, P.; Krol, M. M.; Austrins, L.; Peace, C.; Sleep, B. E.; O'Carroll, D. M.
838 Characterization of nZVI mobility in a field scale test. *Environ. Sci. Technol.* **2014**, *48*,
839 2862–2869.
840 (63) Del Bianco, L.; Fiorani, D.; Testa, A. M.; Bonetti, E.; Savini, L.; Signoretti, S.
841 Magnetothermal behavior of a nanoscale Fe/Fe oxide granular system. *Phys. Rev.*
842 *B* **2002,** *66* (17).

(64) Ezzatahmadi, N.; Ayoko, G. A.; Millar, G. J.; Speight, R.; Yan, C.; Li, J. H.; Li, S. Z.; Zhu, J. X.; Xi, Y. F. Clay-supported nanoscale zero–valent iron composite materials for the remediation of contaminated aqueous solutions: A review. *Chem. Eng. J.* **2017,** *312*, 336–350.
(65) Fan, D. M.; Lan, Y.; Tratnyek, P. G.; Johnson, R. L.; Filip, J.; O'Carroll, D. M.; Garcia, A. N.; Agrawal, A. Sulfidation of iron–based materials: A review of processes and implications for water treatment and remediation. *Environ. Sci. Technol.* **2017,** *51* (22), 13070–13085.
(66) Fu, F. L.; Dionysiou, D. D.; Liu, H. The use of zero–valent iron for groundwater remediation and wastewater treatment: A review. *J. Hazard. Mater.* **2014,** *267*, 194–205.
(67) Grafe, M.; Donner, E.; Collins, R. N.; Lombi, E. Speciation of metal(loid)s in environmental samples by X-ray absorption spectroscopy: A critical review. *Anal. Chim. Acta* **2014,** *822*, 1–22.
(68) Henderson, A. D.; Demond, A. H. Long-term performance of zero–valent iron permeable reactive barriers: A critical review. *Environ. Eng. Sci.* **2007,** *24* (4), 401–423.
(69) Li, L.; Fan, M. H.; Brown, R. C.; Van Leeuwen, J. H.; Wang, J. J.; Wang, W. H.; Song, Y. H.; Zhang, P. Y. Synthesis, properties, and environmental applications of nanoscale iron-based materials: A review. *Crit. Rev. Environ. Sci. Tech.* **2006,** *36* (5), 405–431.
(70) Mukherjee, R.; Kumar, R.; Sinha, A.; Lama, Y.; Saha, A. K. A review on synthesis, characterization, and applications of nano zero valent iron (nZVI) for environmental remediation. *Crit. Rev. Environ. Sci. Tech.* **2016,** *46* (5), 443–466.
(71) Raychoudhury, T.; Scheytt, T. Potential of zerovalent iron nanoparticles for remediation of environmental organic contaminants in water: a review. *Water Sci. Tech.* **2013,** *68* (7), 1425–1439.
(72) Stefaniuk, M.; Oleszczuk, P.; Ok, Y. S. Review on nano zerovalent iron (nZVI): From synthesis to environmental applications. *Chem. Eng. J.* **2016,** *287*, 618–632.
(73) Tosco, T.; Papini, M. P.; Viggi, C. C.; Sethi, R. Nanoscale zerovalent iron particles for groundwater remediation: a review. *J. CleaN. Prod.* **2014,** *77*, 10–21.
(74) Zou, Y. D.; Wang, X. X.; Khan, A.; Wang, P. Y.; Liu, Y. H.; Alsaedi, A.; Hayat, T.; Wang, X. K. Environmental remediation and application of nanoscale zero-valent iron and its composites for the removal of heavy metal ions: A review. *Environ. Sci. Technol.* **2016,** *50* (14), 7290–7304.
(75) Uzum, C.; Shahwan, T.; Eroglu, A. E.; Lieberwirth, I.; Scott, T. B.; Hallam, K. R. Application of zero–valent iron nanoparticles for the removal of aqueous Co^{2+} ions under various experimental conditions. *Chem. Eng. J.* **2008,** *144* (2), 213–220.
(76) Yan, W. L.; Herzing, A. A.; Li, X. Q.; Kiely, C. J.; Zhang, W. X. Structural evolution of Pd–doped nanoscale zero-valent iron (nZVI) in aqueous media and implications for particle aging and reactivity. *Environ. Sci. Technol.* **2010,** *44* (11), 4288–4294.
(77) Liu, A. R.; Liu, J.; Zhang, W. X. Transformation and composition evolution of nanoscale zero valent iron (nZVI) synthesized by borohydride reduction in static water. *Chemosphere* **2015,** *119*, 1068–1074.
(78) Liu, A.; Liu, J.; Han, J.; Zhang, W. X. Evolution of nanoscale zero-valent iron (nZVI) in water: Microscopic and spectroscopic evidence on the formation of nano- and micro-structured iron oxides. *J. Hazard. Mater.* **2017,** *322*, 129–135.
(79) Pullin, H.; Springell, R.; Parry, S.; Scott, T., The effect of aqueous corrosion on the structure and reactivity of zero–valent iron nanoparticles. *Chem. Eng. J.* **2017,** *308*, 568–577.

(80) Pullin, H.; Crane, R. A.; Morgan, D. J.; Scott, T. B. The effect of common groundwater anions on the aqueous corrosion of zero-valent iron nanoparticles and associated removal of aqueous copper and zinc. *J. Environ. Chem. Eng.* **2017,** *5* (1), 1166–1173.

(81) Schoftner, P.; Waldner, G.; Lottermoser, W.; Stoger–Pollach, M.; Freitag, P.; Reichenauer, T. G. Electron efficiency of nZVI does not change with variation of environmental parameters. *Sci. Total Environ.* **2015,** *535*, 69–78.

(82) Tsarev, S.; Collins, R. N.; Fahy, A.; Waite, T. D. Reduced uranium phases produced from anaerobic reaction with nanoscale zerovalent iron. *Environ. Sci. Technol.* **2016,** *50* (5), 2595–2601.

(83) Hwang, Y.; Shin, H. S., Effects on nano zero-valent iron reactivity of interactions between hardness, alkalinity, and natural organic matter in reverse osmosis concentrate. *J. Environ. Sci-China* **2013,** *25* (11), 2177–2184.

(84) Wang, Q. L.; Kanel, S. R.; Park, H.; Ryu, A.; Choi, H. Controllable synthesis, characterization, and magnetic properties of nanoscale zerovalent iron with specific high Brunauer-Emmett-Teller surface area. *J. Nanopart. Res.* **2009,** *11* (3), 749–755.

(85) Liu, T. X.; Li, X. M.; Waite, T. D. Depassivation of aged Fe^0 by divalent cations: Correlation between contaminant degradation and surface complexation constants. *Environ. Sci. Technol.* **2014,** *48* (24), 14564–14571.

(86) Kim, H. S.; Ahn, J. Y.; Hwang, K. Y.; Kim, I. K.; Hwang, I. Atmospherically stable nanoscale zero–valent iron particles formed under controlled air contact: Characteristics and reactivity. *Environ. Sci. Technol.* **2010,** *44* (5), 1760–1766.

(87) Klimkova, S.; Cernik, M.; Lacinova, L.; Filip, J.; Jancik, D.; Zboril, R. Zero-valent iron nanoparticles in treatment of acid mine water from in situ uranium leaching. *Chemosphere* **2011,** *82* (8), 1178–1184.

(88) Ma, X. M.; He, D.; Jones, A. M.; Collins, R. N.; Waite, T. D. Reductive reactivity of borohydride- and dithionite-synthesized iron-based nanoparticles: A comparative study. *J. Hazard. Mater.* **2016,** *303*, 101–110.

(89) Sun, Y. P.; Li, X. Q.; Cao, J. S.; Zhang, W. X.; Wang, H. P. Characterization of zero-valent iron nanoparticles. *Adv. Colloid Interface Sci.* **2006,** *120* (1–3), 47–56.

(90) Lin, K. S.; Chang, N. B.; Chuang, T. D. Fine structure characterization of zero-valent iron nanoparticles for decontamination of nitrites and nitrates in wastewater and groundwater. *Sci. Tech. Adv. Mater.* **2008,** *9* (2).

(91) Wu, C.; Tu, J. W.; Liu, W. Z.; Zhang, J.; Chu, S. Q.; Lu, G. N.; Lin, Z.; Dang, Z. The double influence mechanism of pH on arsenic removal by nano zero valent iron: electrostatic interactions and the corrosion of Fe^0. *Environ. Sci. Nano* **2017,** *4* (7), 1544–1552.

(92) Ma, J. X.; He, D.; Collins, R. N.; He, C. S.; Waite, T. D. The tortoise versus the hare - Possible advantages of microparticulate zerovalent iron (mZVI) over nanoparticulate zerovalent iron (nZVI) in aerobic degradation of contaminants. *Water Res.* **2016,** *105*, 331–340.

(93) Ravel, B.; Newville, M., ATHENA, ARTEMIS, HEPHAESTUS: data analysis for X-ray absorption spectroscopy using IFEFFIT. *J. Synchrotron Rad.* **2005,** *12*, 537–541.

(94) Reardon, E. J.; Fagan, R.; Vogan, J. L.; Przepiora, A. Anaerobic corrosion reaction kinetics of nanosized iron. *Environ. Sci. Technol.* **2008,** *42* (7), 2420–2425.

(95) Zhang, L. N.; Zhou, M. F.; Shao, L. M.; Wang, W. N.; Fan, K. N.; Qin, Q. Z., Reactions of Fe with H_2O and FeO with H_2. A combined matrix isolation FTIR and theoretical study. *J. Phys. Chem. A* **2001,** *105* (29), 6998–7003.

(96) Linderoth, S.; Morup, S.; Bentzon, M. D. Oxidation of nanometer-sized iron particles. *J. Mater. Sci.* **1995**, *30*, 3142–3148.

(97) Cabrera, N; Mott, N. F. Theory of the oxidation of metals. *Rep. Prog. Phys.* **1949**, *12*, 163–184.
(98) Chernavskii, P. A.; Peskov, N. V.; Mugtasimov, A. V.; Lunin, V. V. Oxidation of metal nanoparticles: Experiment and model. Russ. *J. Phys. Chem. B* **2007**, *1* (4), 394–411.
(99) Roosendaal, S. J.; Bakker, J. P. R.; Vredenberg, A. M.; Habraken, F. H. P. M. Passivation of iron oxidation in H_2O and O_2/H_2O mixtures. *Surf. Sci.* **2001**, *494* (3), 197–205.
(100) Grosvenor, A. P.; Kobe, B. A.; McIntyre, N. S. Studies of the oxidation of iron by air after being exposed to water vapour using angle–resolved X-ray photoelectron spectroscopy and QUASES. *Surf. Interface Anal.* **2004**, *36* (13), 1637–1641.
(101) Grosvenor, A. P.; Kobe, B. A.; McIntyre, N. S. Activation energies for the oxidation of iron by oxygen gas and water vapour. *Surf. Sci.* **2005**, *574* (2–3), 317–321.
(102) Sarathy, V.; Tratnyek, P. G.; Nurmi, J. T.; Baer, D. R.; Amonette, J. E.; Chun, C.; Penn, R. L.; Reardon, E. J. Aging of iron nanoparticles in aqueous solution: effects on structure and reactivity. *J. Phys. Chem. C* **2008**, *112*, 2286–2293.
(103) Greenlee, L. F.; Torrey, J. D.; Amaro, R. L.; Shaw, J. M. Kinetics of zero valent iron nanoparticle oxidation in oxygenated water. *Environ. Sci. Technol.* **2012,** *46* (23), 12913–12920.
(104) Dong, H.; Zhao, F.; Zeng, G. M.; Tang, L.; Fan, C. Z.; Zhang, L. H.; Zeng, Y. L.; He, Q.; Xie, Y. K.; Wu, Y. A. Aging study on carboxymethyl cellulose-coated zero-valent iron nanoparticles in water: Chemical transformation and structural evolution. *J. Hazard. Mater.* **2016,** *312*, 234–242.
(105) Dong, H.; Zhao, F.; He, Q.; Xie, Y. K.; Zeng, Y. L.; Zhang, L. H.; Tang, L.; Zeng, G. M. Physicochemical transformation of carboxymethyl cellulose–coated zero-valent iron nanoparticles (nZVI) in simulated groundwater under anaerobic conditions. *Sep. Purif. Tech.* **2017,** *175*, 376–383.
(106) Dong, H.; Jiang, Z.; Deng, J. M.; Zhang, C.; Cheng, Y. J.; Hou, K. J.; Zhang, L. H.; Tang, L.; Zeng, G. M. Physicochemical transformation of Fe/Ni bimetallic nanoparticles during aging in simulated groundwater and the consequent effect on contaminant removal. *Water Res.* **2018**, *129*, 51–57.
(107) Nurmi, J. T.; Tratnyek, P. G.; Sarathy, V.; Baer, D. R.; Amonette, J. E.; Pecher, K.; Wang, C. M.; Linehan, J. C.; Matson, D. W.; Penn, R. L.; Driessen, M. D. Characterization and properties of metallic iron nanoparticles: Spectroscopy, electrochemistry, and kinetics. *Environ. Sci. Technol.* **2005,** *39* (5), 1221–1230.
(108) Liu, Y.; Phenrat, T.; Lowry, G. V. Effect of TCE concentration and dissolved groundwater solutes on NZVI-Promoted TCE dechlorination and H_2 evolution. *Environ. Sci. Technol.* **2007,** *41 (22)*, 7881–7887.
(109) Su, Y. F.; Hsu, C. Y.; Shih, Y. H. Effects of various ions on the dechlorination kinetics of hexachlorobenzene by nanoscale zero–valent iron. *Chemosphere* **2012,** *88* (11), 1346–1352.
(110) Shih, Y. H.; Chen, M. Y.; Su, Y. F. Pentachlorophenol reduction by Pd/Fe bimetallic nanoparticles: Effects of copper, nickel, and ferric cations. *Appl. Catal. B–Environ.* **2011,** *105* (1–2), 24–29.
(111) Fan, J.; Guo, Y. H.; Wang, J. J.; Fan, M. H. Rapid decolorization of azo dye methyl orange in aqueous solution by nanoscale zerovalent iron particles. *J. Hazard. Mater.* **2009,** *166* (2–3), 904–910.
(112) Su, C. M.; Puls, R. W. Nitrate reduction by zerovalent iron: Effects of formate, oxalate, citrate, chloride, sulfate, borate, and phosphate. *Environ. Sci. Technol.* **2004,** *38* (9), 2715–2720.

(113) Karabelli, D.; Uzum, C.; Shahwan, T.; Eroglu, A. E.; Scott, T. B.; Hallam, K. R.; Lieberwirth, I. Batch removal of aqueous Cu^{2+} ions using nanoparticles of zero-valent iron: A study of the capacity and mechanism of uptake. *Ind. Eng. Chem. Res.* **2008,** *47 (14)*, 4758–4764.

(114) Efecan, N.; Shahwan, T.; Eroglu, A. E.; Lieberwirth, I. Characterization of the uptake of aqueous Ni^{2+} ions on nanoparticles of zero-valent iron (nZVI). *Desalination* **2009,** *249 (3)*, 1048–1054.

(115) Zhang, Y. L.; Chen, W.; Dai, C. M.; Zhou, C. L.; Zhou, X. F. Structural evolution of nanoscale zero-valent iron (nZVI) in anoxic Co^{2+} solution: Interactional performance and mechanism. *Sci. Rep.* **2015,** *5*.

(116) Liu, T. X.; Li, X. M.; Waite, T. D. Depassivation of aged Fe^0 by ferrous ions: Implications to contaminant degradation. *Environ. Sci. Technol.* **2013,** *47* (23), 13712–13720.

(117) Kim, H-S.; Ahn, J-Y.; Kim, C.; Lee, S.; Hwang, I. Effect of anions and humic acid on the performance of nanoscale zero-valent iron particles coated with polyacrylic acid. *Chemosphere* **2014**, *113*, 93–100.

(118) Glavee, G. N.; Klabunde, K. J.; Sorensen, C. M.; Hadjipanayis, G. C. Chemistry of borohydride reduction of iron(II) and iron-(III) ions in aqueous and nonaqueous media - formation of nanoscale Fe, FeB, and Fe_2B powders. *Inorg. Chem.* **1995**, *34*, 28–35.

(119) McCormick, M. L.; Adriaens, P. Carbon tetrachloride transformation on the surface of nanoscale biogenic magnetite particles. *Environ. Sci. Technol.* **2004**, *38*, 1045–1053.

(120) Carpenter, E. E.; Calvin, S.; Stroud, R. M.; Harris, V. G. Passivated iron as core-shell nanoparticles. *Chem. Mater.* **2003**, *15*, 3245–3246.

(121) Bae, S.; Gim, S.; Kim, H.; Hanna, K. Effect of $NaBH_4$ on properties of nanoscale zero-valent iron and its catalytic activity for reduction of p-nitrophenol. *Appl. Catal. B: Environ.* **2016**, *182*, 541–549.

(122) Hua, Q.; Huang, W. Chemical etching induced shape change of magnetite microcrystals. *J. Mater. Chem.* **2008**, *18*, 4286– 4290.

(123) Dong, H. R.; Lo, I. M. C. Influence of humic acid on the colloidal stability of surface-modified nano zero-valent iron. *Water Res.* **2013,** *47* (1), 419–427.

(124) Hydutsky, B. W.; Mack, E. J.; Beckerman, B. B.; Skluzacek, J. M.; Mallouk, T. E. Optimization of nano- and microiron transport through sand columns using polyelectrolyte mixtures. *Environ. Sci. Technol.* **2007,** *41* (18), 6418–6424.

(125) Lee, C.; Keenan, C. R.; Sedlak, D. L. Polyoxometalate–enhanced oxidation of organic compounds by nanoparticulate zero-valent iron and ferrous ion in the presence of oxygen. *Environ. Sci. Technol.* **2008,** *42 (13)*, 4921–4926.

(126) Kim, H. H.; Lee, H.; Kim, H. E.; Seo, J.; Hong, S. W.; Lee, J. Y.; Lee, C. Polyphosphate-enhanced production of reactive oxidants by nanoparticulate zero-valent iron and ferrous ion in the presence of oxygen: Yield and nature of oxidants. *Water Res.* **2015,** *86*, 66–73.

(127) Keenan, C. R.; Sedlak, D. L. Ligand-enhanced reactive oxidant generation by nanoparticulate zero-valent iron and oxygen. *Environ. Sci. Technol.* **2008,** *42* (18), 6936–6941.

(128) Kim, E. J.; Kim, J. H.; Azad, A. M.; Chang, Y. S. Facile Synthesis and Characterization of Fe/FeS Nanoparticles for Environmental Applications. *ACS Appl. Mater. Inter.* **2011,** *3* (5), 1457–1462.

(129) Scott, T. B.; Dickinson, M.; Crane, R. A.; Riba, O.; Hughes, G. M.; Allen, G. C. The effects of vacuum annealing on the structure and surface chemistry of iron nanoparticles. *J. Nanopart. Res.* **2010,** *12* (5), 1765–1775.

(130) Riba, O.; Barnes, R. J.; Scott, T. B.; Gardner, M. N.; Jackman, S. A.; Thompson, I. P. Enhanced reactivity of nanoscale iron particles through a vacuum annealing process. *J. Nanopart. Res.* **2011,** *13* (10), 4591–4601.

(131) Gong, Y. Y.; Gai, L. S.; Tang, J. C.; Fu, J.; Wang, Q. L.; Zeng, E. Y. Reduction of Cr(VI) in simulated groundwater by FeS-coated iron magnetic nanoparticles. *Sci. Total. Environ.* **2017,** *595*, 743–751.

(132) Cao, Z.; Liu, X.; Xu, J.; Zhang, J.; Yang, Y.; Zhou, J. L.; Xu, X. H.; Lowry, G. V. Removal of antibiotic florfenicol by sulfide–modified nanoscale zero-valent iron. *Environ. Sci. Technol.* **2017,** *51 (19)*, 11269–11277.

(133) Li, J.; Zhang, X.; Sun, Y.; Liang, L.; Pan, B.; Zhang, W.; Guan, X. Advances in sulfidation of zerovalent iron for water decontamination. *Environ. Sci. Technol.* **2017,** *51* (23), 13533–13544.

(134) Liang, F.; Fan, J.; Guo, Y. H.; Fan, M. H.; Wang, J. J.; Yang, H. Q. Reduction of nitrite by ultrasound–dispersed nanoscale zero-valent iron particles. *Ind. Eng. Chem. Res.* **2008,** *47* (22), 8550–8554.

(135) Rasheed, Q. J.; Pandian, K.; Muthukumar, K., Treatment of petroleum refinery wastewater by ultrasound-dispersed nanoscale zero-valent iron particles. *Ultrason. Sonochem.* **2011,** *18* (5), 1138–1142.

(136) Mikhailov, I. ; Mandal, A. R.; Kotov, S.; Kuznetsov, D. A new ultrasound-assisted method of wastewater treatment by air–stable nanosized zero-valent iron. *Adv. Electrochem*. **2014,** *1*, 1–4.

(137) Geiger, C. L.; Ruiz, N. E.; Clausen, C. A.; Reinhart, D. R.; Quinn, J. W. Ultrasound pretreatment of elemental iron: kinetic studies of dehalogenation reaction enhancement and surface effects. *Water Res.* **2002,** *36 (5)*, 1342–1350.

(138) Yang, Z. L.; Wang, X. L.; Li, H.; Yang, J.; Zhou, L. Y.; Liu, Y. D. Re-activation of aged-ZVI by iron–reducing bacterium Shewanella putrefaciens for enhanced reductive dechlorination of trichloroethylene. *J. Chem. Technol. Biot.* **2017,** *92* (10), 2642–2649.

(139) Lu, X.; Li, M.; Tang, C.; Feng, C.; Liu, X. Electrochemical depassivation for recovering Fe^0 reactivity by Cr(VI) removal with a permeable reactive barrier system. *J. Hazard. Mater.* **2012**, 213–214, 355–360.

(140) Liu, Y.; Lowry, G. V. Effect of particle age (Fe^0 content) and solution pH on NZVI reactivity: H_2 evolution and TCE dichlorination. *Environ. Sci. Technol.* **2006**, *40*, 6085–6090.

Table 1. Representative studies reporting passivation byproducts of NZVI under different experimental conditions.

Synthesis method	Reaction condition	O_2 condition	Reaction time	Passivation byproduct	Refs
Fe^{3+} + $NaBH_4$	complete mixing	oxygenated water + oxic condition	3 d	Lepi	38
$FeCl_3$•$6H_2O$ + $NaBH_4$	no mixing	oxygenated water + oxic condition	5 d	Magn/Magh	77
			10 d	Ferr/ Magn/Magh	
			90 d	Lepi	
$Fe_2(SO_4)_3 \cdot 6H_2O$ + $NaBH_4$	Cl^- (10 mM)	water + oxic condition	2 h	Magn/Magh	80
			2 w	Akag/ Magn/Magh	
			16 w	Lepi /Magn/Magh	
$Fe_2(SO_4)_3 \cdot 6H_2O$ + $NaBH_4$	HCO_3^- (10 mM)	water + oxic condition	2 h	Magn/Magh	80
			8 w	Goet/ Magn/Magh	
$Fe_2(SO_4)_3 \cdot 6H_2O$ + $NaBH_4$	NO_3^- (10 mM)	water + oxic condition	2 h	Magn/Magh	80
			16 h	Magn/Magh	
$Fe_2(SO_4)_3 \cdot 6H_2O$ + $NaBH_4$	SO_4^{2-} (10 mM)	water + oxic condition	2 h	Magn/Magh	80
			2 w	Lepi/Magn/Magh	
			16 w	Goet/Lepi/Magn/Magh	

RNIP 10-DP, product from Toda Kogyo Corp., Reduction of Fe(III) oxides by H_2	NO_3^- (10 mM) + rotated end-over-end at 22 °C	deaerated water + anoxic condition	6 m	Magn	33
RNIP 10-DP, product from Toda Kogyo Corp. Reduction of Fe(III) oxides by H_2	PO_4^{2-} (10 mM) + rotated end-over-end at 22 °C	deaerated water + anoxic condition	1 m 6 m	Magn Vivi/Schw	33
NANOFER 25DS, product from NANO IRON (inorganic S based coating), Reduction of Fe(III) oxides by H_2	Synthetic groundwater (Cl^- (1.95 mN), HCO_3^- (1.14 mN), NO_3^- (0.15 mN), SO_4^{2-} (0.44 mM))	deaerated water + anoxic condition		Magn	117
NANOFER 25 DS, product from NANO IRON (inorganic S based coating), Reduction of Fe(III) oxides by H_2	Synthetic groundwater (Cl^- (1.95 mN), HCO_3^- (1.14 mN), NO_3^- (0.15 mN), SO_4^{2-} (0.44 mM)) + Humic acid (2.5 mg L^{-1})	deaerated water + anoxic condition		Iron carbonate hydroxide hydrate	117
$FeCl_3 \cdot 6H_2O + NaBH_4$	microcystin-LR (5.0 mg L^{-1}) + PO_4^{2-} (0.4 mM) + added H_2O_2 (6.6 mM)	water + oxic condition	4 h	Vivi	34
$FeCl_3 \cdot 6H_2O + NaBH_4$	microcystin-LR (5.0 mg L^{-1}) + humic acid (0.4 mM) + added H_2O_2 (6.6 mM)	water + oxic condition	4 h	Lepi	34

$FeCl_3$•$6H_2O$ + $NaBH_4$	microcystin-LR (5.0 mg L^{-1}) + oxalate (0.4 mM) + added H_2O_2 (6.6 mM)	water + oxic condition	4 h	Magn/Lepi	34
NANOFER STAR, product from NANO IRON	synthetic groundwater with an ionic strength of 15 mM	groundwater + anoxic condition	6 d	Amak/Goet/Magn	81
Fe^{3+} + $NaBH_4$	As(V) (2 mg L^{-1}) + synthetic groundwater at pH 5	groundwater + oxic condition	30 d 60 d	Magn/Magh/Lepi/Hema Lepi	18
Fe^{3+} + $NaBH_4$	synthetic groundwater at pH 9	groundwater l IU+ oxic condition	30 d 60 d	Magn/Magh Magn/Magh	18
$FeSO_4$•$7H_2O$+ $NaBH_4$	U(VI):Fe(0)=1:21, 50 mM NaCl, 5.8 mM $NaHCO_3$ and 1 mM $CaCl_2$, synthetic groundwater at pH 7	groundwater + anoxic condition	3 d 12 m	Chuk Chuk/Magn	82
$FeCl_3$•$6H_2O$ + $NaBH_4$	NO_3^- (100 mg L^{-1}), HCO_3^- (5 g L^{-1})	deaerated water + anoxic condition	3 h	Gree(CO_3)	83
$FeCl_3$•$6H_2O$ + $NaBH_4$	NO_3^- (100 mg L^{-1}), Humic acid (1 g L^{-1}; DOC = 320 mg L^{-1})	deaerated water + anoxic condition	3 h	Magn	83
$FeCl_3$•$6H_2O$ + $NaBH_4$	complete mixing at 300 rpm	deaerated water + anoxic condition	3 d	Wust/Goet/Lepi	78

$FeSO_4•7H_2O + NaBH_4$ + carboxymethyl cellulose	$Na_2S_2O_4$ (0.1 M), rolling on a hematology mixer at 15 rpm and pH 7.2	deaerated water + anoxic condition	2 d	Mack	35
$FeCl_2•4H_2O + NaBH_4$	1 μM $H^{14}COO^-$, pH 6.2–8.3	oxygenated water + oxic condition	1 d	Side	36
RNIP 10-DS, product from Toda America, Inc. Reduction of Fe(III) oxides by H_2	Dry powder	deaerated water + anoxic condition	<20 d	Mixed-valent Fe(II) and Fe(III) oxide	102
RNIP 10-DP, product from Toda Kogyo Corp. Reduction of Fe(III) oxides by H_2	Alkaline slurry, pH =10.6	deaerated water + anoxic	2 y	Magn	140

Lepi: Lepidocrocite ($\overline{\gamma\text{-}Fe^{III}OOH}$), Magn: Magnetite ($\overline{Fe^{II}{}_1{}^{III}{}_2O_4}$), Magh: Maghemite ($\overline{\gamma\text{-}Fe^{III}{}_2O_3}$), Ferr: Ferrihydrite ($\overline{5Fe^{III}{}_2O_3•9H_2O}$), Akag: akageneite ($\beta\text{-}Fe^{III}OOH$), Schw: schwertmannite ($Fe^{III}16O_{16}(OH,SO_4)_{12–13}·10–12H_2O$), Wust: wüstite ($Fe^{II}O$), Amak: amakinite ($Fe^{II}(OH)_2$), Goet: goethite ($\alpha\text{-}Fe^{III}OOH$), Hema: hematite ($\alpha\text{-}Fe^{III}{}_2O_3$), Vivi: vivianite ($Fe^{II}{}_3(PO_4)_2·8H_2O$), Gree($CO_3$): Carbonate green rust: $[Fe^{II}4Fe^{III}{}_2(OH)_{12}][CO_2·H_2O]$, Mack: mackinawite ($Fe^{II}S$), Side: siderite ($Fe^{II}CO_3$)

Figure captions

Figure 1. STEM images and XEDS maps showing NZVI oxidation by oxygen-containing water (a) fresh NZVI, (b) after 30 min and (c) 5 h reaction. (d) The corresponding graph shows the proportions of Fe present as either Fe(0), ferrihydrite or lepidocrocite as determined by linear combination fitting of EXAFS data. Reproduced with permission from ref 36, Copyright 2016, American Chemical Society.

Figure 2. TEM images of NZVI after reaction with water under anoxic conditions at (a) 25 and (b) 80 ^{o}C, respectively, and the long-term corrosion results at (c) 25 and (d) 80 ^{o}C, showing the proportions of Fe present as either Fe(0), $Fe(OH)_2$, or magnetite as determined by ^{57}Fe Mössbauer Spectroscopy. Reproduced with permission from ref 39, Copyright 2014, American Chemical Society.

Figure 3. A conceptual model on the passivation of NZVI in water showing that the main passivation byproducts include wustite (FeO), goethite (α-FeOOH) and akaganeite (β-FeOOH) under anoxic conditions while crystalline lepidocrocite (γ-FeOOH) with acicular-shaped structures forms under oxic conditions. Reproduced with permission from ref 78, Copyright 2017, Elsevier.

Figure 4. Results of TEM (a and c) and XRD (b and d) of NZVI showing the passivation of NZVI over one month at pH 8 in 5 and 25 mN HCO_3^- suspensions. The XRD diffraction patterns associated with specific mineral phases are noted as α-Fe for Fe(0), M for magnetite, GR for carbonate green rust, and ICH for iron carbonate hydroxide. Reproduced with permission from ref 4, Copyright 2012, American Chemical Society.

Figure 5. Schematic illustration showing the cation-induced depassivation process of aged micro-scale ZVI by Fe(II) dissolution of sheet or shell structures upon metal complexation on the NZVI surface. Cations: M^{2+}: Ba^{2+}, Sr^{2+}, Ca^{2+}, Mg^{2+}, Mn^{2+}, Co^{2+}, Fe^{2+}, Ni^{2+}, Zn^{2+}, Pb^{2+}, and Cu^{2+}. Reproduced with permission from ref 85, Copyright 2014, American Chemical Society.

Figure 6. Schematic illustrations showing the NZVI applications, typical passivation process of NZVI at different conditions, and environmental significance of the passivation.

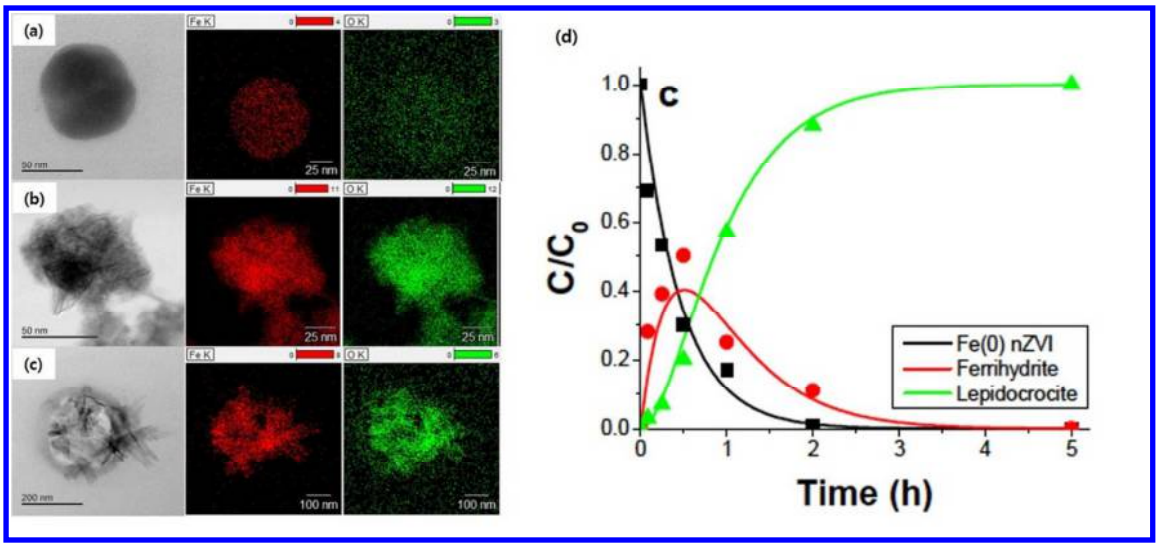
(a)
(b)
(c)
(d)
Fe K
O K
25 nm
100 nm
C/C0
Time (h)
Fe(0) nZVI
Ferrihydrite
Lepidocrocite

Figure 1.

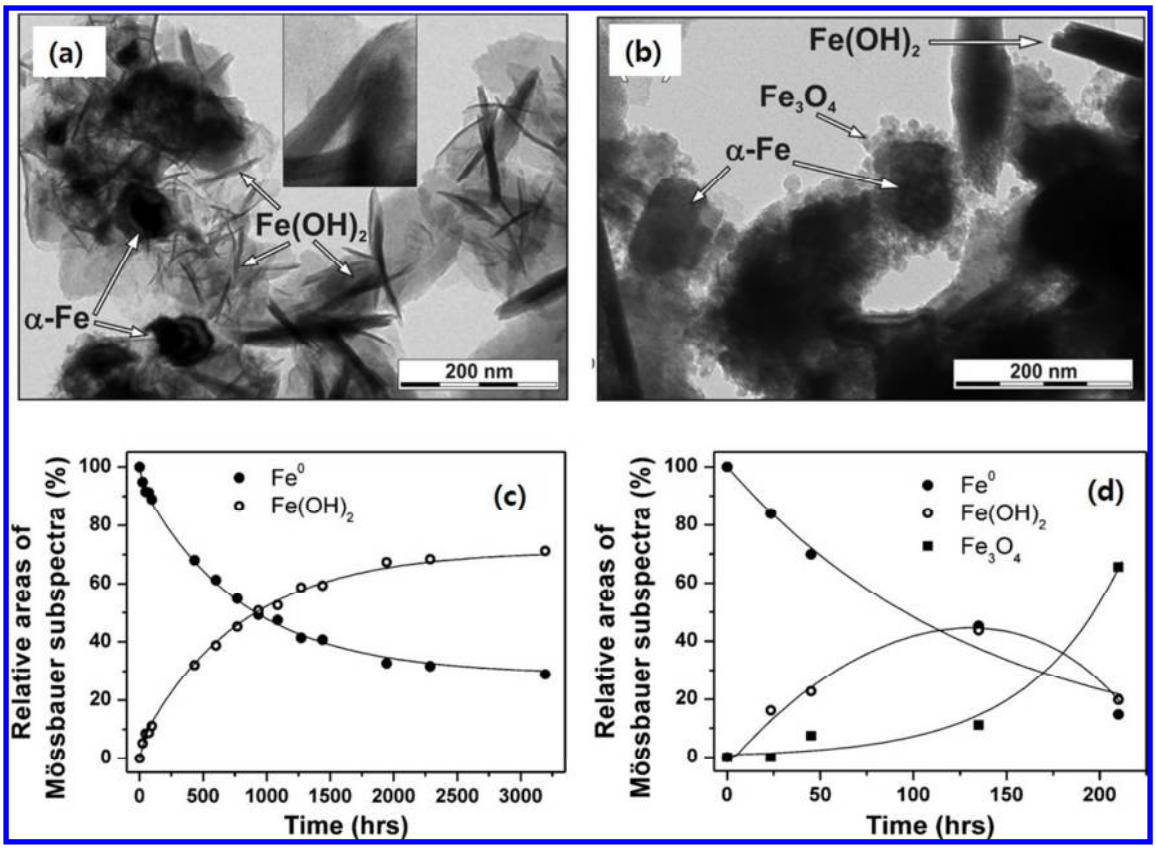
(a)
Fe(OH)2
α-Fe
200 nm
(b)
Fe(OH)2
Fe3O4
α-Fe
200 nm
Relative areas of Mössbauer subspectra (%)
Fe0
Fe(OH)2
(c)
Time (hrs)
Relative areas of Mössbauer subspectra (%)
Fe0
Fe(OH)2
Fe3O4
(d)
Time (hrs)

Figure 2.

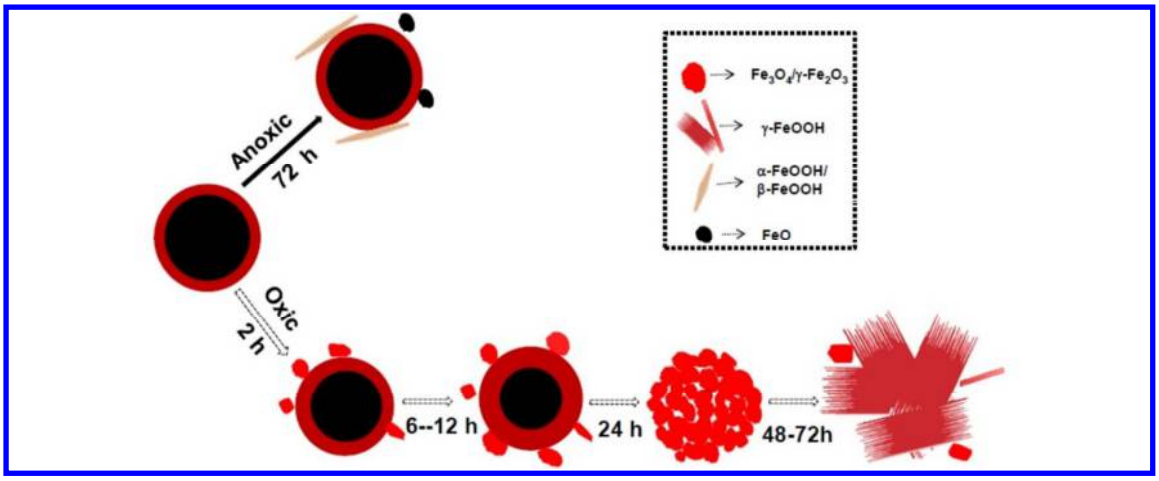
Anoxic
72 h
Oxic
2 h
6--12 h
24 h
48-72h
Fe_3O_4/γ-Fe_2O_3
γ-FeOOH
α-FeOOH/
β-FeOOH
FeO

Figure 3.

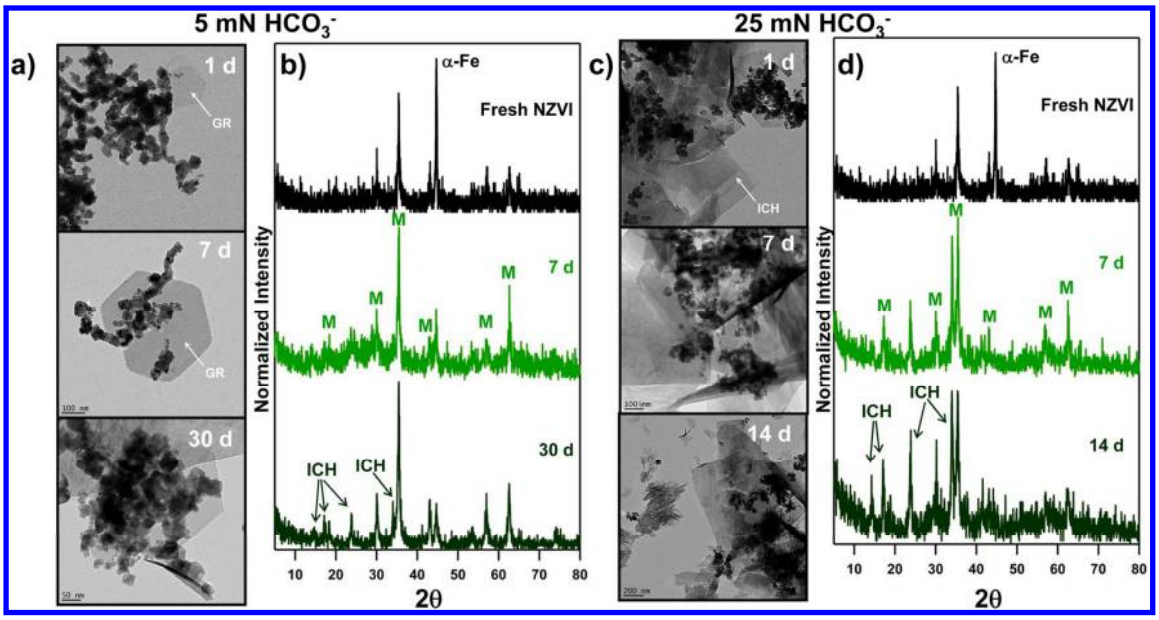
5 mN HCO3-
25 mN HCO3-
a)
b)
c)
d)
1 d
7 d
30 d
14 d
GR
ICH
α-Fe
Fresh NZVI
M
ICH
Normalized Intensity
2θ
10 20 30 40 50 60 70 80

Figure 4.

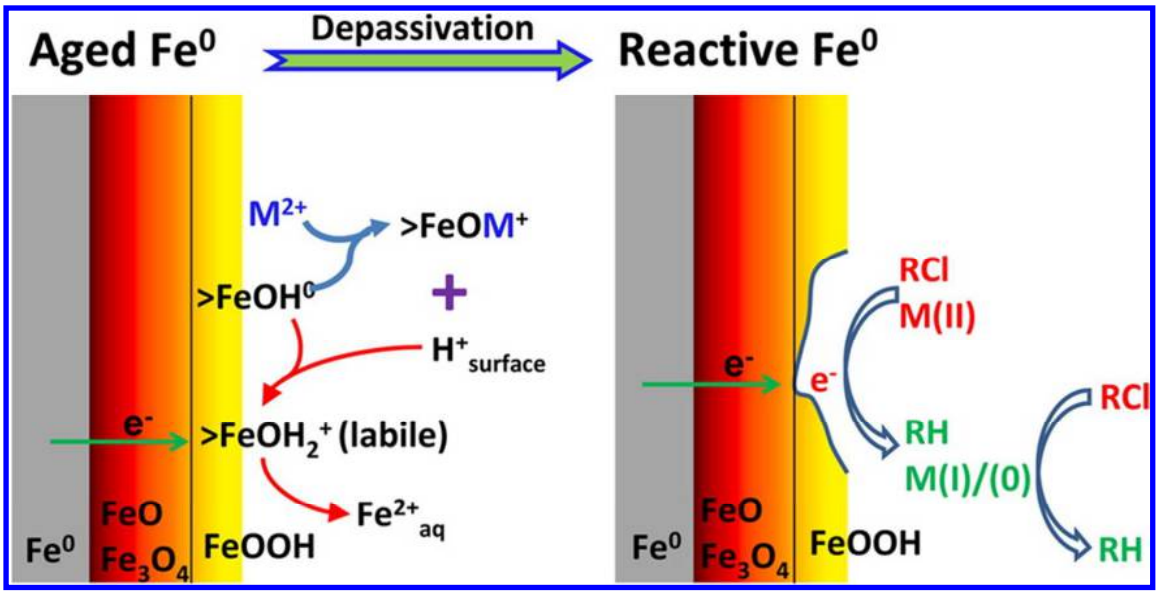
Aged Fe0
Depassivation
Reactive Fe0
M2+
>FeOM+
>FeOH0
+
H+surface
e-
>FeOH2+ (labile)
Fe2+aq
Fe0
FeO
Fe3O4
FeOOH
RCl
M(II)
e-
RH
M(I)/(0)
RCl
RH

Figure 5.

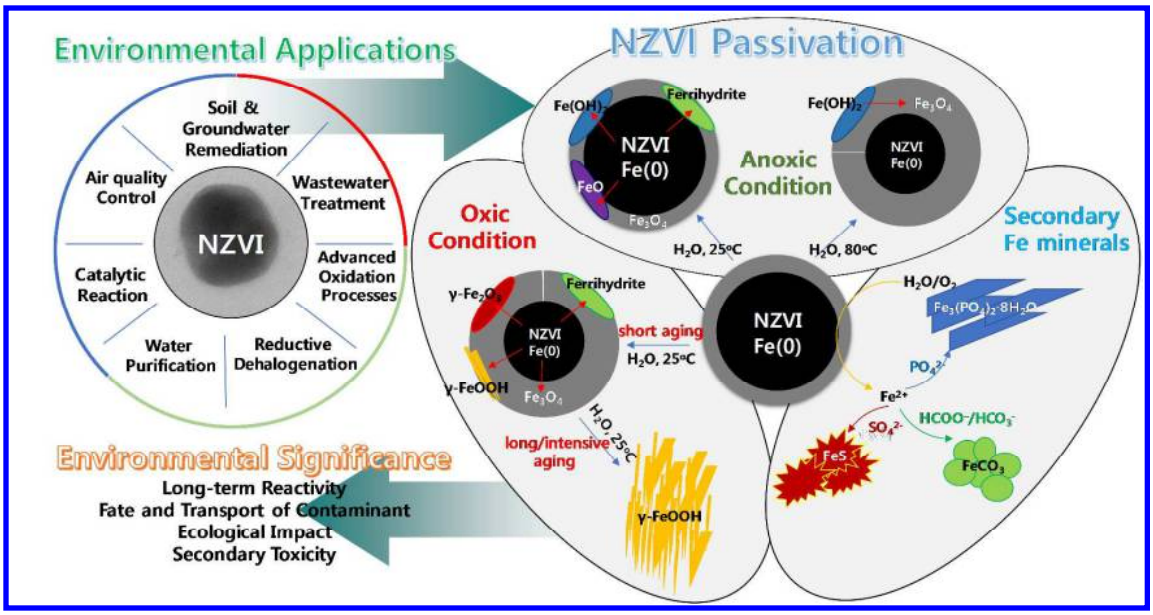
Environmental Applications
Soil & Groundwater Remediation
Wastewater Treatment
Advanced Oxidation Processes
Reductive Dehalogenation
Water Purification
Catalytic Reaction
Air quality Control
NZVI
Environmental Significance
Long-term Reactivity
Fate and Transport of Contaminant
Ecological Impact
Secondary Toxicity
NZVI Passivation
Fe(OH)2
Ferrihydrite
NZVI Fe(0)
FeO
Fe3O4
H2O, 25°C
H2O, 80°C
Anoxic Condition
Oxic Condition
γ-Fe2O3
γ-FeOOH
short aging
long/intensive aging
Secondary Fe minerals
H2O/O2
Fe3(PO4)2·8H2O
PO4 2-
Fe2+
SO4 2-
FeS
HCOO-/HCO3-
FeCO3

Figure 6.

TOC

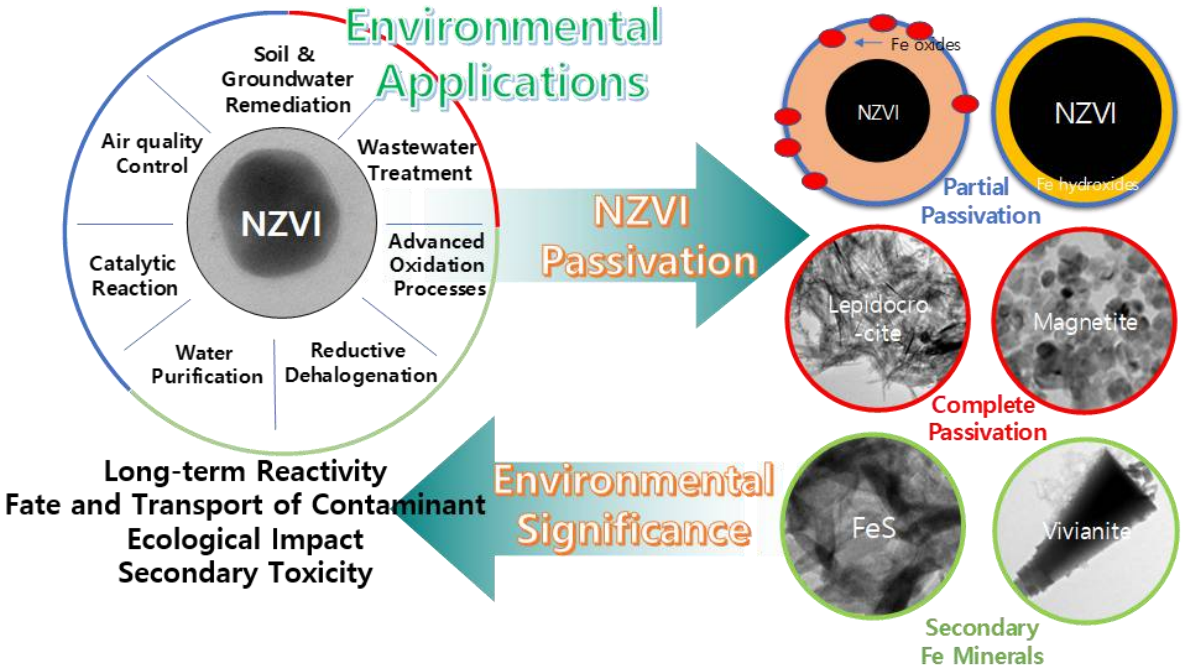
Environmental Applications
Soil & Groundwater Remediation
Wastewater Treatment
Advanced Oxidation Processes
Reductive Dehalogenation
Water Purification
Catalytic Reaction
Air quality Control
NZVI
NZVI Passivation
Fe oxides
NZVI
NZVI
Fe hydroxides
Partial Passivation
Lepidocro -cite
Magnetite
Complete Passivation
FeS
Vivianite
Secondary Fe Minerals
Environmental Significance
Long-term Reactivity
Fate and Transport of Contaminant
Ecological Impact
Secondary Toxicity